

Gaia-DR2 asteroid observations and INPOP planetary ephemerides

P. Deram¹ · A. Fienga^{1,2} · A. K. Verma³ · M. Gastineau² · J. Laskar²

Received: date / Accepted: date

Abstract Keywords Celestial mechanics – ephemerides – gravitation – methods: numerical, data analysis

We used the INPOP19a planetary ephemerides to perform the orbital adjustment of 14099 asteroids based on Gaia-DR2 observations, and compare for 23 of them the resulting orbits to radar data. As Gaia-DR2 has been processed using the planetary ephemeris INPOP10e, the primary goal of this paper is to confirm the portability of the data when using an updated version of the solar system model. In particular, we point out the fact that the Gaia satellite positions - provided with respect to the INPOP10e solar system barycenter - must be corrected when using another planetary ephemeris . We also present a convenient least square formalism that only handles small matrices and allows the adjustment of global parameters, such as masses. In order to check the consistency of the Gaia observations with other types of observations, we perform an orbital adjustment in combining Gaia and radar range observations for 23 objects, together with a careful post-fit analysis including an estimation of the Gaia systematic errors. Finally, we show that to ensure the combined use of Gaia angular DR2 observations and radar ranging, a more developed than firstly proposed dynamical modeling is required together with the addition of the systematic Gaia bias in the fit procedure. These results give promising directions for the next Gaia delivery, Gaia-DR3.

1 Asteroid observations in Gaia-DR2

In 2013, the Gaia astrometric satellite of the European Space Agency (ESA) was launched at the Lagrange point L2 for surveying the stellar population of the Milky way (Gaia Collaboration et al, 2016) with an unparalleled precision of astrometric accuracy (down to 24 μ arcseconds) . Parallel to this main mission

GéoAzur, CNRS, Observatoire de la Côte d’Azur, Université Côte d’Azur, 250 Av. A. Einstein, Valbonne, 06560, France · IMCCE, Observatoire de Paris, PSL University, CNRS, Sorbonne Université, 77 avenue Denfert-Rochereau, Paris, 75014, France · University of California, Los Angeles, CA, USA

, representing a billion of observations, the Gaia capability of observing small extended targets was also employed to provide a large survey of detected Solar System objects.

In 2018, as part of the Gaia Data Release 2 (Gaia-DR2), were released the positions of about 14 099 known asteroids based on 1 977 702 observations acquired during the first 22 months of the mission between August 5, 2014 and May 23, 2016 (Gaia Collaboration et al, 2018a). Gaia-DR2 includes mainly asteroids from the Main Belt and Near-Earth, and Kuiper belt objects. The archived positions are given in the Gaia specific coordinates AL and AC (respectively along and across the Gaia scan directions), with an optimal range of brightness G between 12 and 17 where the accuracy in the AL direction reaches the milliarcsecond level (mas). As the errors in the AC direction is considerably larger, the information provided by Gaia is essentially 1D. However, due to the large variety of orientations and scan directions covered by Gaia over time (a minimal number of 12 transits per object were requested for DR2), the AL direction alone provides strong orbital constraints (Gaia Collaboration et al, 2018b).

Gaia Collaboration et al (2018b) presented the main step of the solar system objects data processing and performed a first orbital fit based on Gaia observations only. They included 16 massive perturbers in their dynamical model and used JPL's DE431 planetary ephemeris (Folkner et al, 2014) to access the positions of the planets. In the AL direction, they reported a mean residual of 0.05 mas with a standard deviation of 2.14 mas which is in accordance with the announced accuracy. For objects brighter than $G=13$, the same order of accuracy was also reported in the AC direction as a full 2D window was transmitted (with a larger pixel size in AC). However, as expected, for objects with $G>13$, the error in AC remained considerably larger (of about 600 mas) as all pixels were binned to a single window.

These promising results were based only on 22 months of observations and pose great opportunities for future research as a release of nearly 100 000 objects is expected with the Gaia-DR3, and a time coverage of 5 years. However, as the Gaia-DR2 observations were processed using the planetary ephemerides INPOP10e (Fienga et al, 2012, 2013) and as planetary ephemerides have evolved since 2013, it is worth checking the compatibility of these observations when using an updated version of Solar system ephemeris, for investigating mainly the potential impact of model dependencies and the portability of the released observations.

This planetary ephemeris model dependency operates at different steps and levels during the processing of the Gaia observations (Fienga et al, 2016). A prior knowledge of the position and velocity vectors of the satellite with respect to the barycenter of the Solar system (SSB) is for example necessary in order to apply the aberration corrections to the source apparent positions and to determine the stellar parallaxes with the proper scale. It is also required to process the astrometric data into BCRS (Barycentric celestial reference System) with its origin at the SSB, and its reference directions tied to the International Celestial Reference System (ICRS).

The goal of this paper is first to check the compatibility of the Gaia observations processed with INPOP10e, when we adjust with the latest version of INPOP. Secondly, we seek to validate our adjustment method in anticipation of the huge amount of observations that will be available with DR3 by confronting estimated orbits to very accurate radar observations..

Table 1 Differences between INPOP10e and INPOP19a planetary ephemerides. The first part of the table provides a breakdown of the differences based on dynamic modeling and adjustment. The second part of the table summarizes additional data added since INPOP10e that was used to construct INPOP19a. More details can be found in Sect 2.1 and 2.2

	INPOP10e Fienga et al (2012, 2013)	INPOP19a Fienga et al (2019a,c) Di Ruscio et al (2020b)
Dynamical modeling		
Main belt asteroid perturbations	343 + 1 ring	343
TNO perturbations	none	3 rings
Moon libration and core rotation	approximated for fluid core, no inner core	full for fluid core, no inner core
Fit and estimated parameters		
total number of estimated parameters	210	402
asteroid masses	152	343
ring mass	main belt	TNO
Dataset Time interval	1913:2010	1924:2017
INPOP19a Additional datasets	Planets	Time coverage
Messenger	Mercury	2011:2014
Cassini	Saturn	2004:2017
Juno	Jupiter	2016:2019
MEX	Mars	2014:2017
MRO	Mars	2010:2014

In Sect. 2, we provide an overview of the differences between INPOP10e and INPOP19a ephemerides (Fienga et al, 2019b,a). The details of the inversion method used in this study are discussed in Sect. 3. The results of the joint analysis that includes Gaia satellite and ground-based radar data are provided in Sect. 4. In Sect. 5, we analyse the impact of the weighting schema and perturber list on the obtained residuals.

2 Planetary ephemerides

The INPOP planetary ephemeris (Intégrateur Numérique Planétaire de l’Observatoire de Paris) was built in 2006 (Fienga et al, 2008b) and has become a reference for science in solar system dynamics and fundamental physics. INPOP numerically integrates the orbits of the Sun, planets, the Moon, and selected asteroids. The positions and velocities of these bodies are estimated using more than 150,000 observations such as lunar laser ranging, spacecraft tracking, and ground-based observations. The INPOP ephemerides are regularly updated following the constant improvement of the Solar system model and the addition of new observations. They are distributed at <http://www.imcce.fr/inpop>. (Fienga et al, 2008b, 2011a, 2015a, 2019c). We present two ephemerides in the following subsections: INPOP10e, used in the Gaia data processing, and INPOP19a, the latest version used in this paper for the asteroid orbital adjustment.

2.1 INPOP10e

A first version of INPOP, INPOP06, was published in 2008 (Fienga et al, 2008a) with a dynamical model and a fit procedure very close to the JPL reference

ephemerides of the time. The addition of new observational data and the evolution of the dynamical models and adjustment techniques led to the successive release of the INPOP series, followed by INPOP08 (Fienga et al, 2009), INPOP10a (Fienga et al, 2011b), and INPOP10e (Fienga et al, 2013), developed for the Gaia mission and released in 2013.

Besides providing the user with positions and velocities of the planets and the Moon, INPOP provides also the rotation angles of the Earth and the Moon as well as TT-TDB in accordance with the recommendations of the International Astronomical Union (IAU) in terms of time scale, metric (relativistic equation of motion), and Sun gravitational mass (with a fixed astronomical unit (au)). In INPOP10e, 152 asteroid masses were also estimated using a sophisticated procedure based on a bounded least square associated with prior sigma and solar plasma corrections (Verma et al, 2013).

In accordance with the Gaia mission and IAU requirements, the link with the ICRF was maintained by the use of VLBI differential observations of planetary spacecrafts relative to the ICRF sources. The combination of such VLBI observations with spacecraft navigation provides the planet positions relative to the ICRF sources at the level of accuracy of the VLBI space mission localization (typically milliarcsecond). With the INPOP10e version, such a tie was sustained by VLBI tracking data of inner planets and outer planets - especially Mars, VEX, and Cassini observations - with an accuracy of about 1 mas for the period 2003-2013.

In terms of observations, the INPOP10e was the first INPOP version to benefit from flyby observations in addition to the classical ground-based optical ones. For the inner planets, MEX and VEX radiometric and VLBI observations were crucial for Mars and Venus orbits. Uranus and Neptune orbits were also benefited from the use of positions deduced from the Voyager 2 (two flybys). For Mercury, three positions were deduced from the Messenger flybys while for Jupiter, five Juno flybys were used.

Typically the maximum difference between INPOP10e and the contemporary JPL's ephemeris - DE420 (Folkner, 2010) - is sub-km for barycentric positions of the inner planets. For Jupiter, the expected accuracy of INPOP10e can not be better than the postfit residuals obtained by comparison to flyby positions which are as large as 2 kilometers. However, in INPOP10e, the Jupiter fitting interval ends in 2001 so no secular trend could have been calibrated during the Gaia period. The situation is similar for Saturn, as its orbit has been highly improved thanks to the few Cassini observations. The corresponding residuals in geocentric distances decreased from several hundred kilometers for the precedented INPOP versions to few tens of meters with INPOP10e but only on the available Cassini period of time (Jones et al, 2014). For Uranus and Neptune, the DPAC requirement (Fienga et al, 2016) of an uncertainty in positions of few kilometers over the Gaia period was not reached because of the limited number of observations of these bodies.

2.2 INPOP19a

Since the INPOP10e release in 2013, updated versions of INPOP have been regularly delivered: INPOP13c in 2013 with an improvement of the Mercury orbit based on MESSENGER radio tracking data (Verma et al, 2014; Fienga et al, 2014), INPOP15a with new Cassini radio tracking data (Fienga et al, 2015b),

INPOP17a with an important improvement of the dynamical modeling of the Earth-Moon system (Viswanathan, 2017) and finally, INPOP19a (Fienga et al, 2019b,a). The main differences between INPOP10e and INPOP19a are presented in Table 1

In terms of dataset, INPOP19a benefits from two major updates: the inclusion of the first nine perijove passes of Juno around Jupiter, and reanalysis of Cassini radio tracking around Saturn (Di Ruscio et al, 2020a) by extending the time coverage from 2014 to 2017 (including the final phase of the mission and Titan flyby gravity solutions).

Concerning the dynamical modeling, the main difference is coming from the introduction of a set of three rings centered at the SSB, located in the ecliptic plane at the distances of 39.4, 44 and 47.5 AU and representing the gravitational influences of Trans-Neptunian Objects. The total mass of the three ring has been adjusted to a mass of $0.061 \pm 0.001 M_{\oplus}$ (Di Ruscio et al, 2020a; Fienga et al, 2019b). Consequently, Cassini Grand Finale residuals improved significantly. In addition, 343 Main Belt asteroids were integrated and their masses estimated using a Monte Carlo procedure described in Fienga et al (2019a). This leads to an important improvement in the accuracy of the Mars orbit. The well known masses of nine binary TNOs were also included in the dynamical model.

Comparing INPOP19a to INPOP10e, we found a difference on the SSB position (based on the SSB-Earth vector) of about 95 km over the Gaia period (see Fig. 1). This difference is mainly due to a pure geometrical effect: the addition of 9 massive TNOs (Fienga et al, 2019b) between INPOP10e and INPOP19a with planetesimal masses and large semimajor axes (40 au) creates a leverage effect on the SSB position. This difference is not constant in time and exhibits both an oscillation (with an amplitude of about 270 meters) with respect to the Earth orbit period and a regular drift (see Fig. 1), showing that a dynamical difference exists between the two models. As the Gaia satellite positions and velocities in Gaia-DR2 are given with respect to the INPOP10e SSB, it is clear that specific cares must be taken when substituting INPOP10e with INPOP19a or any other ephemeris. Without correction, the 95 km difference implies an error of about one hundred times bigger than the 1 mas accuracy expected by Gaia, and cannot be absorbed during the adjustment of the asteroid initial conditions to the Gaia data. Generally, the position of the SSB depends on the masses and positions of all the objects included in the ephemerides, implying a strong model dependency of the satellite positions and velocities provided by the Gaia release. We draw attention to the fact that the Gaia team (Gaia Collaboration et al, 2018b) did not apply any correction to the Gaia position when analyzing data with DE431. A quick comparison shows a discrepancy of about 240 meters in the SSB position relative to the Earth between INPOP10e and DE431 over the Gaia period. In the worst case, this error implies a 0.3 mas difference on the angular position of an object at 1 au from the satellite. Presumably, due to the small number of transits and the short time-span of Gaia-DR2, this error is easily absorbed during the fit of the initial conditions of the asteroids - that is why it had remained invisible up to now - but it would become critical with the future DR3. We believe that the Gaia satellite positions would benefit from being provided in the Earth-centered reference frame to avoid this model dependency.

In addition to the planetary adjustment, we added to INPOP19a the positions and velocities of the 14099 asteroids observed by Gaia and provided by Gaia-DR2.

The asteroid orbits are integrated with the same code and integrator as INPOP19a using the same initial conditions but with a Newtonian formalism, including the perturbations of the Sun and main planets but with a reduced number of perturbing asteroids compared to INPOP19a. In terms of perturbing asteroids, for a sake of comparison, we chose the same list of 16 perturbers as in Gaia Collaboration et al (2018b). The masses of the 16 perturbers included in the dynamical model are presented in table 2 and were extracted from Fienga et al (2019a)

Table 2 List of the 16 perturbing asteroids used in Gaia Collaboration et al (2018b) with their corresponding mass in INPOP19a. Stars indicate the five objects that were also observed by Gaia and available in DR2.

Asteroid number	GM
-	$[10^{18} AU^3.d^{-2}]$
1	139643.532
2	32613.272
3	3806.229
4	38547.977
6	986.372
7	1833.933
10	11954.671
15	3936.840
16	3088.668
29	2103.023
52*	2308.950
65	2990.906
87*	2726.311
88*	0.055
511*	6637.430
704*	4737.367

Finally, we verify that the asteroid orbital improvements resulting from the Gaia observations on the massive asteroids included in the INPOP19a modeling do not have any significant impact on the previously obtained planetary orbits, as such no iteration is needed between asteroid and planetary adjustment procedure.

We also check that no residual rotation has been observed between the planetary ephemerides obtained with and without the Gaia observations. On Table 3, one can find Euler angles fitted over the two ephemerides for different cases, depending which planetary orbits are considered. If all the orbits including the outer planet ones are considered, the mis-alignment of the INPOP reference frame axis (by definition, the ICRF, without considering the VLBI observation uncertainties) with the Gaia reference frame (GRF) is not statistically significant with standard deviation smaller than 1 mas. However if we consider only the orbits fitted over very accurate observations such as the inner planets, Jupiter and Saturn, then the Euler angles turn out to have significant values but at the level of few μas . This is far below the uncertainty of the alignment between DR2 GRF and ICRF3 of about 20 to 30 μas as obtained by (Gaia Collaboration et al (2018a)). We can then conclude to a good alignment of the INPOP reference axis relative to the DR2 GRF.

Table 3 Euler angles fitted by comparing two planet ephemerides only different by the asteroid orbits used for computing their perturbations on the planet orbits: one being fitted over the Gaia DR2 and one obtained from the astorb data base.

	θ	ψ	ϕ
	μas	μas	μas
All planets	-98 ± 1508	1.0 ± 45	253 ± 3971
Inner planets	1.16 ± 0.20	-0.08 ± 0.62	-1.50 ± 0.150
Inner planets + Jupiter	1.23 ± 0.16	-1.0 ± 0.22	-0.128 ± 0.69
Inner planets + Jupiter + Saturn	1.83 ± 0.80	1.057 ± 0.053	-0.23 ± 2.56
Outer planets	-55 ± 629	-30 ± 495	373 ± 5051

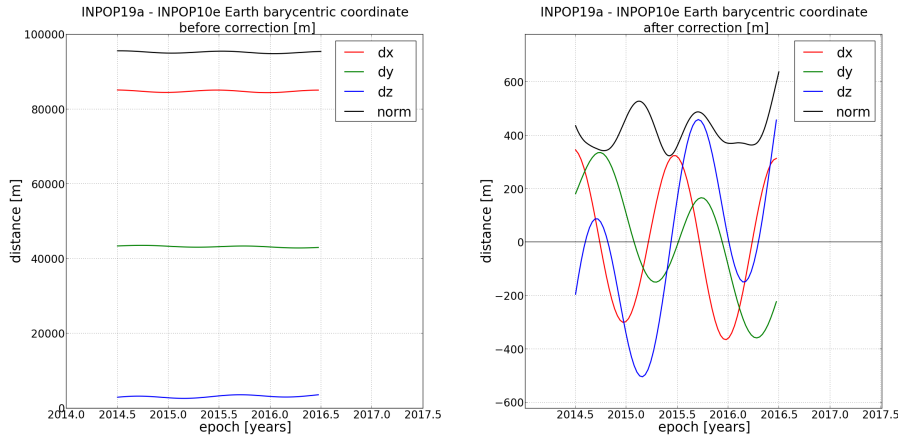


Fig. 1 SSB-Earth vector difference between INPOP19a and INPOP10e in Cartesian coordinates. *Left*: before correction by a constant vector. *Right*: After correction by a constant vector based on the mean of the difference. We find $dx=84.3$ km, $dy=44.8$ km, $dz=3.6$ km.

3 Asteroid orbits with Gaia-DR2

3.1 Method

We integrated 14099 orbits with INPOP using the procedure described previously and computed observables as given in Gaia Collaboration et al (2018b). Concerning the positions of the Gaia satellite, as the SSB is shifted between INPOP10e and INPOP19a (see Sect. 2.2), we apply a preliminary transformation from Gaia barycentric positions to Gaia geocentric ones before switching to the new ephemeris. The idea is to consider the Earth-Gaia vector provided with the DR2 Solar system modeling (INPOP10e) as an invariant, independent from the model. This is justified because the satellite positions are usually based on ground-based telemetry. Therefore, for each Gaia observation, we simply report the Gaia geocentric position obtained with INPOP10e to INPOP19a, and we then avoid the model dependency intrinsically present in the barycentric coordinates. At this step, after a first comparison between computed observables and Gaia observations, an optimisation of the asteroid orbital initial conditions is required. The

$$W = \begin{bmatrix} W_1 & & & & \\ & W_2 & & 0 & \\ & & \ddots & & \\ & & & 0 & W_i \\ & & & & & W_n \end{bmatrix} \quad (6)$$

,where ξ_1 and W_1 are respectively the residual vector and weight matrix for the p perturbers and ξ_i , W_i for the i th perturbed body (starting at $i=2$). For inverting such a system, a strategy of block-wise inversion using the Schur complement (Zhang, 2005) was performed, and a global solution for the normal equations is given by:

$$\begin{cases} \Delta x_1 = -COV(J_1^T W_1 \xi_1 + B) \\ \Delta x_i = -(J_i^T W_i J_i)^{-1} J_i^T W_i (\xi_i - P_i x_1) \quad \text{for } (i \geq 2) \end{cases} \quad (7)$$

,with:

$$COV = (J_1^T W_1 J_1 + A)^{-1} \quad (8)$$

$$A = \sum_{i=1}^n C_i P_i \quad B = \sum_{i=1}^n C_i \xi_i \quad (9)$$

and

$$C_i = P_i^T W_i [1 - J_i (J_i^T W_i J_i)^{-1} J_i^T W_i] \quad (10)$$

In the context of the expected amount of data that will be released with the Gaia DR3, the solution given in Eq. 7 is convenient because it only handles small matrices that can be computed in an iterative way (see Eq. 9). We note that if all P_i are set to zero (no perturbers), Eq. 7 is then equivalent to n independent normal equations where each asteroid is adjusted without taking into account the others.

In practice, the P_i perturbing terms (caused by the small variations of the perturber orbital initial conditions) are very small and the solution provided by a system where all the asteroids are independent would be very close to the one found with this rigorous method accounting for the perturbations of main perturbers. This could be easily seen by looking at the second equation of 7, where the solution is the classical one applied to a residual corrected from the perturbation induced by the perturbers.

A quick estimation of the impact of the position uncertainty of a perturber on a perturbed orbit could be computed by estimating the derivative of the acceleration with respect to the position. A perturber position error dr causes an acceleration error proportional to dr/r , where r is the distance between the perturber and the perturbed asteroid. For a 100 km error at 1 au the relative effect $\delta a/a$ is smaller than 10^{-6} . As a comparison, the error in the mass of the perturber (in this case, a few percent) is likely to be much larger, so the effect of the perturber trajectory errors on perturbed residuals is unlikely to be significant unless the mass is estimated as well. However, as this formalism is adapted for the adjustment of

any global parameter (it requires only to add few columns in the matrix P_i), it will be particularly convenient in the perspective of Gaia DR3, where the masses of the biggest objects would be probably measurable though their perturbations on the trajectories of multiple asteroids (Mouret et al, 2008)

3.2 Results of the Gaia fit

Fig. 2 presents the residuals obtained before and after the fit of the 14099 asteroids using INPOP19a. The fitted dataset includes 1 977 702 observations from 287940 transits. 98% of the AC residuals fall in the interval ± 800 mas . 96% of the AL residuals fall in the interval ± 5 mas and 53% are at the sub-milliarcsec level. A comparison of these results with those published in Gaia Collaboration et al (2018b) is presented in Table 4. Both results are highly consistent , at least in the AL direction. The peak around 0, visible in the right-hand side figure of Fig. 2 for the AC direction, is related to the magnitude dependency of the residuals and gathers objects brighter than $G=13$ for which the accuracy in the AC direction reaches the milliarcsecond level. This behavior is also apparent in Fig 3, showing the residual distribution as a function of the G magnitude.

Similarly to Figs. 27 and 28 in Gaia Collaboration et al (2018b), Fig. 4 shows the absolute values of the mean and standard deviations per transit. These representations are more convenient than the one used on Fig. 2, as they put into evidence the existence of systematic errors at a transit level (classically, the means of the residuals per transit) and provide a better estimation of the debiased residuals (classically, the standard deviations of the residuals per transit), to be compared with the expected random errors. However, given the small number of observations per transit (≈ 7) and the relative magnitude between random and systematic errors (for $G>13$, the random error is at least 40 times greater than the systematic one in the AC direction), it is clear that in our case, the mean values are strongly influenced by random errors and cannot be taken as accurate estimations of the systematic ones. Typically, for n values issued from a Gaussian distribution with a variance σ^2 , the standard deviation of the mean is given by σ/\sqrt{n} . In the AC direction, where the the random error roughly equals to 300 mas and where there are an average of 7 observations par transit, we find a standard error of about 110 mas on the mean, which is much more than the expected systematic error (up to 10 mas). This could clearly be seen on Fig 4, looking at the mean residuals per transit in the AC direction, where a value of about 100 mas is obtained for $G>13$. The transition at $G=13$ is another consequence of the strong dependency of the mean residuals with respect to the random errors as no transition is expected in the systematic errors. Finally, the mean residuals per transit cannot be taken as a good estimator of the systematic error in the AC direction as it provides a value with a uncertainty bigger than the expected value itself ($S/N < 1$). The situation is different in the AL direction. In this direction, for $G<17$, the random error is expected to be smaller than the systematic error so that the mean residuals per transit give an estimation of the systematic error with $S/N > \sqrt{N}$. For an average number of observation per transit of about 7, the $S/N > 2.6$. Thus, the top row of Fig 4 demonstrates the existence of a systematic error smaller than 1 mas in the AL direction, and the bottom figures of Fig 4 shows the clear increment of the AL

Table 4 Means and standard deviations of the Gaia Post-fit residuals in the AC/AL directions.

	AL		AC	
	mean mas	std mas	mean mas	std mas
This work	0.08	2.12	17.1	294.5
Gaia Collaboration et al (2018b)	0.05	2.14	-	-

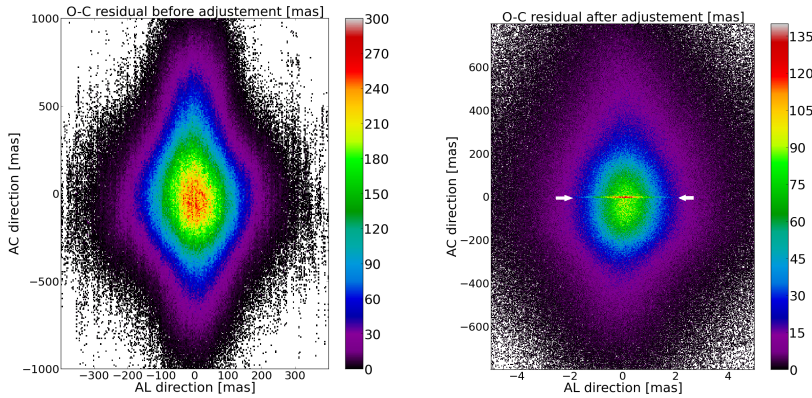


Fig. 2 Density plot of the residuals in the (AL,AC) plane expressed in milliarcsecond. Left panel: before the adjustment of the initial conditions. Right pane: after the adjustment of the initial conditions. The colorbar and the axis range were chosen to be directly comparable with Fig.19 of Gaia Collaboration et al (2018b). The white arrows point the over-density created by residuals of asteroids with $G < 13$.

random errors with the magnitude, the submilliarcsecond accuracy being reached for $G < 17$.

Finally, the correlation between the estimated systematic errors in AL and AC directions must be taken into account in the analysis of the post-fit residuals. The approach discussed in this paper and used by Gaia Collaboration et al (2018b) was insufficient, since a rigorous estimation of systematic bias and debiased residuals was required to compare their values to the expected random and systematic errors.

4 Post-fit analysis and comparisons with radar observations

4.1 Method

4.1.1 Post-fit analysis

To check the accuracy of the orbits obtained after the adjustment with Gaia observations, we carefully analyse the post-fit residuals including the estimation of the Gaia systematic errors. We estimate the systematic bias β_i by minimizing the Eq 11 such as:

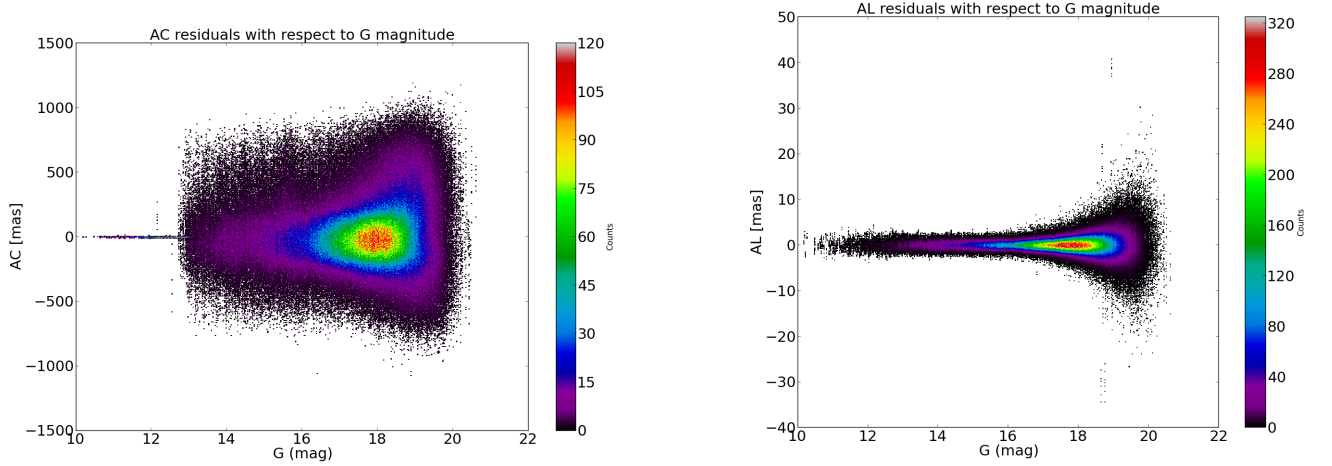


Fig. 3 Density plot of the residuals in AL and AC with respect to the magnitude G after the adjustment of the initial conditions.

$$S = \sum_{i=1}^n \sum_{j=1}^{m_i} (\xi_{ij} - \beta_i)^T W_{ij} (\xi_{ij} - \beta_i) + \sum_{i=1}^n \beta_i^T V_i \beta_i \quad (11)$$

n is the number of transits for the considered object, m_i is the number of (α, δ) observations in the transit i , ξ_{ij} is the j th residual of the transit i , W_{ij} is the random weight matrix for the j th observation of the i th transit, taken as the inverse of the random covariance matrix, β_i is the adjusted systematic error for the transit i , and V_i its weight matrix taken as the inverse of the systematic covariance matrix provided by the DPAC. The second term of the sum in Eq 11 tends to minimize the estimated systematic bias according to the DPAC covariance matrices, whereas the first term of the sum tends to reduce Gaia debiased residuals in accordance with the announced random errors. Therefore, the minimization of Eq 11 leads to an optimization of the so-called "Bias variance trade-off".

After convergence achieved and systematic biases estimated, we examine the three most relevant χ^2 values. The first one accounts for the systematic errors by considering the sum:

$$\chi_{sys}^2 = \sum_{i=1}^n \beta_i^T V_i \beta_i \quad (12)$$

whereas the second and the third χ^2 deal with the random errors respectively in the AL and AC directions. χ_{sys}^2 measures the compatibility of the estimated systematic bias with the one given by DPAC. We rotated each (α, δ) highly correlated Gaia observations into the (AL, AC) plane where longitudinal and cross directions are essentially non correlated and can then be separated into two independent batches. The same transformation is applied to β and Gaia random covariance matrix to create two diagonal and independent matrices with diagonal

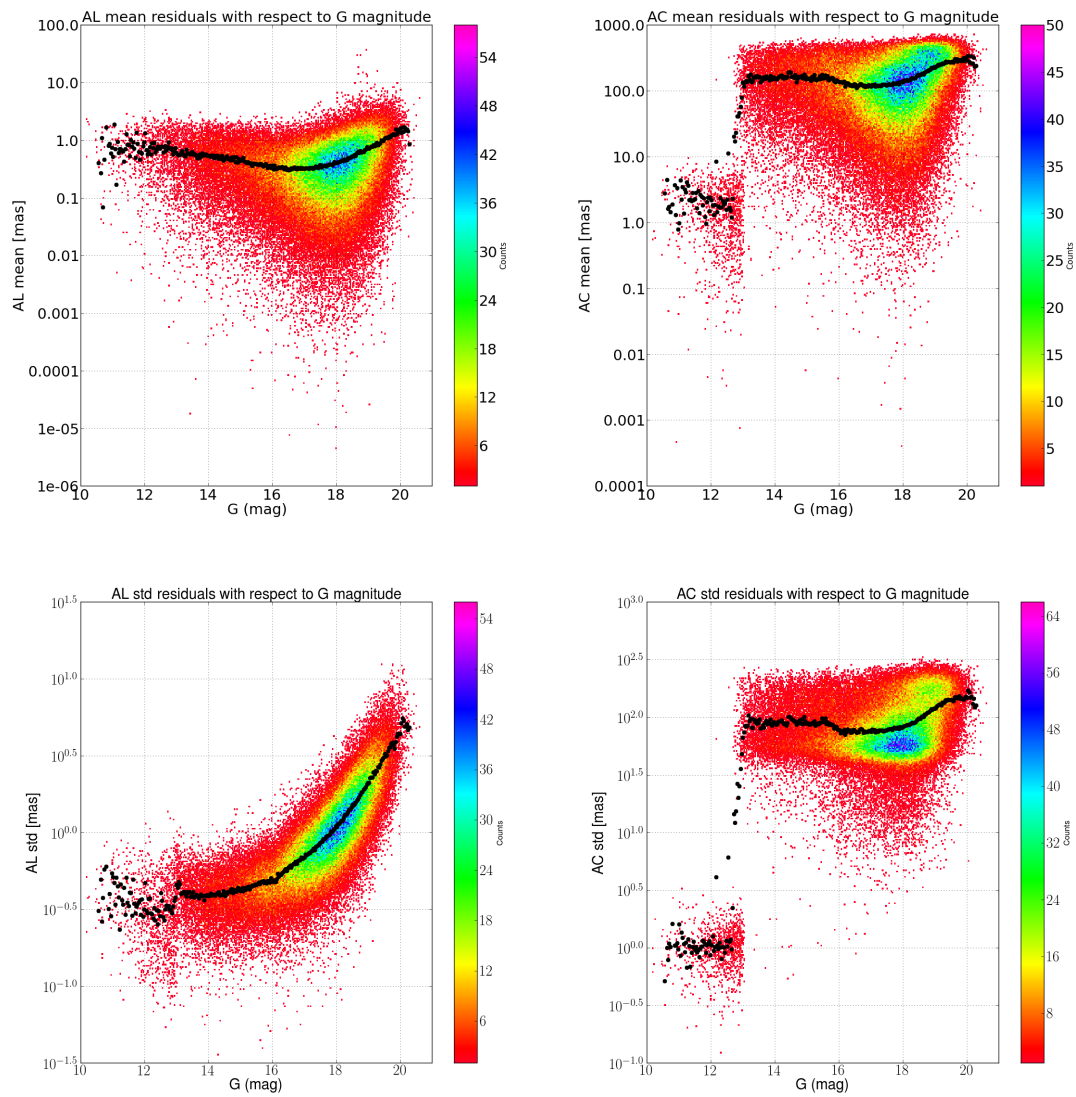


Fig. 4 Density plots of the mean residuals (first row) per transit in AL and AC with respect to the magnitude G after the adjustment of the initial conditions and density plots of the standard deviation of the residuals (second row) per transit in AL and AC with respect to the magnitude G after the adjustment of the initial conditions.

terms equal to $\sigma^2[AL]$ and $\sigma^2[AC]$ respectively. We indicate with $\xi[AL]$ and $\beta[AL]$ ((respectively $\xi[AC]$ and $\beta[AC]$)) the part of the residuals and of the bias related to the AL axis (respectively AC). Two separated χ^2 can then be considered:

$$\chi^2[AL]_{random} = \sum_{i=1}^n \sum_{j=1}^{m_i} \frac{(\xi[AL]_{ij} - \beta[AL]_i)^2}{(\sigma^2[AL]_{ij})} \quad (13)$$

$$\chi^2[AC]_{random} = \sum_{i=1}^n \sum_{j=1}^{m_i} \frac{(\xi[AC]_{ij} - \beta[AC]_i)^2}{(\sigma^2[AC]_{ij})} \quad (14)$$

The goodness of the fit is evaluated using two statistical values derived from the obtained χ^2 (Eq 12, 13, and 14): the Survival rate (SVR) and the Standard error of the regression (SER). The Survival rate is the probability that a real-valued random variable following the χ^2 statistics takes a value greater than the obtained χ^2 . It is computed using the following formula:

$$SVR(\chi^2, k) = 1 - F(\chi^2, k) \quad (15)$$

where F is the cumulative distribution function of a χ^2 statistics with k degrees of freedom:

$$F(\chi^2, k) = \frac{\gamma(\frac{k}{2}, \frac{\chi^2}{2})}{\Gamma(\frac{k}{2})} \quad (16)$$

Γ is the Gamma function and γ the lower incomplete one. Usually, for large k and a residual in perfect accordance with the corresponding standard deviation, $\chi^2=k$ and $SVR=50\%$.

The standard error of the regression (SER) is defined as the multiplicative factor that must be applied to the expected error to obtain a SVR of 50% for the considered residuals. For large k it could be simply computed as the squared root of the reduced χ^2 . A value greater than 1 indicates that the error is underestimated (or the residual is too big) whereas a SER smaller than 1 indicates a SVR bigger than 50 % with a probable overestimation of the error. In the case of SVR estimated for the systematic bias with χ^2_{sys} , a SVR bigger than 50% indicates that the estimated bias is consistent with the one given by DPAC when a SVR close to 0, indicates that the estimated systematic bias has 0 probability of being explained by the DPAC value. In this case, the systematic bias may have absorbed some unmodeled signature.

4.1.2 Comparisons with radar ranging observations

To validate the quality of the obtained orbits, we also extend our dataset with radar range observations available at <https://ssd.jpl.nasa.gov/?radar>. Spanning from 1993 to 2019, a total of 141 radar ranging observations were available for 23 asteroids also observed by Gaia and listed in Table 5. The choice of radar ranging observations in comparison with a more abundant database such as optical angular ground-based observations is justified for 2 reasons: first, we need to compare observations of equivalent accuracy to GAIA DR2 in order to detect potential inconsistencies between the two databases. The radar observations bring also the

benefit of providing out-of-plane and distance informations that are complementary to Gaia angular measurements (α, δ). Second, at this level of accuracy, the use of optical ground-based observations (especially those obtained before 2000) is challenging as they are usually very heterogeneous (different observatories, periods, star-catalogs etc) with poorly known accuracies (see for example Carpino et al (2003); Chesley et al (2010); Farnocchia et al (2015); Vereš et al (2017)). A rigorous treatment of such a database is beyond the scope of this study.

We adjust the orbits of the 23 objects of Table 5 on both Gaia and radar measurements. As we are only working with few individual cases known as perturbed objects, it is relevant to consider them as independent objects from the fit point-of-view. The perturbations induced by the p perturbers are still included in the dynamical modeling but their initial conditions are not re-estimated as they were already fitted with Gaia observations in section 3.

It is equivalent to not include the perturbing matrices P_i in Eq. 4 and to work with J_i matrices extended to radar observations. Therefore, for each of the selected asteroid, the classical least square solution is found using the following combined matrices:

$$W = \begin{bmatrix} W_{Gaia} & 0 \\ 0 & W_{radar} \end{bmatrix} \quad (17)$$

$$J = \begin{bmatrix} J_{Gaia} \\ J_{radar} \end{bmatrix} \quad (18)$$

$$\xi = \begin{bmatrix} \xi_{Gaia} \\ \xi_{radar} \end{bmatrix} \quad (19)$$

where J_{radar} and J_{Gaia} are the Jacobian matrices accounting respectively for the radar and Gaia observations, ξ is the residual matrix that includes Gaia and radar residuals. W_{Gaia} is the weight matrix for the Gaia observations. As in Section 3.1, W_{Gaia} is computed as the inverse of the random covariance matrix provided by the DPAC. W_{radar} , the radar weight matrix, is computed as the inverse of the formal variance errors of the related observations. This error is provided in the JPL file as a standard-error on the round-trip delay. Those values are conservative and also account for the uncertainties on the asteroid shapes. Uncertainties range from few kilometers for the older observations to tens of meters for the most recent.

Finally a χ^2 is computed for the radar residuals, as well as a SVR and a SER using:

$$\chi^2[radar] = \xi_{radar}^T W_{radar} \xi_{radar} \quad (20)$$

4.2 Results

Table 6 shows the Gaia residual post-fit analysis for the solution adjusted on Gaia observations only, obtained in Section 3. Among 23 asteroids, only one (3200 Phaeton) was rejected due to its zero systematic SVR (in practice, $<0.01\%$) with $SER > 2$. Phaeton extremely elongated and chaotic orbit (Galushina and Sambarov, 2019) could explain these extreme values. For (1620), (68216) and (2062), the SVR of 0.23 %, 0.23% and 2.16% respectively in the AL direction are suspicious and

Table 5 Gaia and radar datasets for the 23 selected objects. Each Gaia observation accounts for a pair (α, δ) . The orbital coverage is the ratio between the Gaia observation period and the orbital one.

properties: Asteroid:	Number of observations:		Gaia Orbital coverage	Radar Observations epoch
	Radar	Gaia	[ratio]	[year]
53	1	204	0.35	2002
105	2	116	0.40	1988
216	1	143	0.28	1999
253	1	182	0.39	2001
393	1	122	0.37	2000
433	4	52	0.88	2012, 2019
654	12	55	0.41	1988, 2002
1620	3	82	1.16	1983, 1994
1685	7	102	0.78	1988, 2012, 2016
2062	5	69	1.64	2012, 2013, 2014, 2015
2063	7	22	1.21	1996, 2012, 2015
2100	8	33	1.0	2000, 2003, 2016, 2019
3103	1	65	0.99	1996
3200	8	118	1.03	2007, 2017
4183	1	122	0.34	2000
4769	8	117	0.79	1989, 2012
7889	2	45	0.4	2005
10115	10	103	0.71	1999
11066	4	117	0.49	2004
16834	1	41	0.79	2000
66391	37	24	2.04	2001, 2019
68216	5	24	0.39	2009
68950	12	48	1.4	2003, 2006, 2016, 2019

indicate less than 5% of chance that the values of their AL residuals are only due to Gaia AL random errors. For all other objects, the SVRs are greater than 7% for all the directions, confirming the goodness of the fit obtained in Section 3. We also check that most of the constraint is supported by the AL direction, as the SVR for AC remains considerably larger (20 asteroids out of 23 have an AL SVR greater than 80%). Based on the analysis of 23 objects, it appears that the use of a dynamical model with 16 perturbers and a weight matrix based on random error is sufficient to adjust the asteroid orbits using Gaia observations only. However, because Gaia DR2 only covers 22 months of observations, the success of the adjustment is not sufficient for concluding on the reliability of the obtained orbit and its compatibility with other available observations.

The results of the orbital adjustment on both Gaia and radar are presented on Table 7. The study of the SVR shows that for 13 out of 23 objects ((253), (393), (433), (1620), (1685), (2062), (2063), (2100), (3200), (4769), (11066), (66391) and (68950)), the simple combination of radar and Gaia does not lead to acceptable residuals. For all these 13 objects, the radar residuals are greater than the expected error ($SER > 3$ and up to 165) and for 6 of the mentioned 13 ((1620), (2100), (3200), (4769), (66391) and (68950)), the obtained systematic error is also bigger than expected, leading to a SVR of 0 %. The asteroids (53) and (105) must probably be also rejected as their radar SVR fall to 0.09 % and 1.23% respectively. For 7 asteroids out of 23 ((216), (654), (3103), (4183), (7889), (10115), (16834)), the adjustment on both Gaia and radar measurements is a success as we obtain radar

Table 6 Gaia post-fit residuals based on Gaia data alone. The results are based on a dynamical model with 16 perturbers and a weighting schema based on random error only (similar to Gaia Collaboration et al (2018b)).

properties: Asteroid:	Gaia residuals:						Radar passthrough:		
	AL		AC		Systematic		One-way		
	SER -	SVR %	SER -	SVR %	SER -	SVR %	SER -	SVR %	RMSE km
53	0.98	100	0.71	100	0.22	100	15.2	0	153.6
105	0.94	82	0.52	100	0.18	100	2.6	1	45
216	0.87	98.9	0.39	100	0.41	100	14.6	0	73.6
253	0.78	100	0.27	100	0.14	100	92.7	0	562
393	0.94	82.5	0.4	100	0.19	100	18	0	200.6
433	1.08	21.5	0.67	100	0.1	100	11.9	0	22.54
654	1.14	7.5	0.35	100	0.26	100	64.2	0	1345
1620	1.23	0.23	0.83	98.6	0.43	100	438.4	0	224.7
1685	0.97	65.1	0.57	100	0.36	100	24.4	0	69.7
2062	1.18	2.16	1.01	43.6	0.26	100	74	0	27.4
2063	0.66	99.2	0.53	100	0.21	100	4389	0	1527
2100	1.01	47.0	0.25	100	0.03	100	2519	0	1310
3103	0.87	92.9	1.01	44.3	0.19	100	51	0	51.6
3200	1.1	7.1	0.44	100	2.39	0	2465	0	1412
4183	1.04	27.3	0.52	100	0.28	100	3466	0	1401
4769	1.03	31.8	0.94	80.3	0.31	100	2695	0	339
7889	1.04	36.3	0.57	100	0.02	100	4770	0	2381
10115	0.95	75	0.84	99.1	0.41	100	164336	0	20947
11066	0.94	83.6	0.65	100	0.21	100	175.4	0	63.12
16834	0.98	56.3	0.64	100	0.08	100	310.8	0	377.1
66391	0.84	87.8	0.6	99.9	0.28	100	9251	0	482
68216	1.44	0.23	0.64	99.6	0.02	100	2787	0	758
68950	0.94	72	1	49.7	0.26	100	4261	0	1992

SVR>15% and Gaia SVR>7%. Moreover, for all of these 7 asteroids, the Gaia residuals were not impacted by the extension of the dataset to radar observations, as the Gaia SVRs are roughly the same on Table 6 and Table 7. The case of (68216) is ambiguous as the Gaia AL SVR is small (SVR=0.23%) but constant whether or not the radar measurements are included into the orbital adjustment. Our capability to obtain good radar residuals for (68216) without degrading the Gaia ones could indicate that, in this case, the small Gaia SVR is due more to Gaia data themselves rather than our dynamical model.

Finally, even if the orbital adjustment on Gaia observations only could be considered as a success (Table 6), it is clearly not the case when considering both Gaia and radar measurements (Table 7). In order to understand if the apparent incompatibility between Gaia and radar is due to the data themselves or to our adjustment method, we explore in the next section the impact of two hypotheses: the use of only 16 perturbers in the dynamical model, and the neglect of the systematic errors in the weighting schema.

Table 7 Analysis of the Gaia post-fit residuals in case of an adjustment on both Gaia and radar, using a dynamical model with 16 perturbers and a weighting schema based on random error only.

properties: Asteroid:	residuals:								
	Gaia						Radar		
	AL		AC		Systematic		One-way		
	SER -	SVR %	SER -	SVR %	SER -	SVR %	SER -	SVR %	RMSE km
53	0.98	64.6	0.71	100	0.22	100	4.92	0.09	49.7
105	0.94	82	0.51	100	0.18	100	2.52	1.23	44
216	0.87	98.9	0.39	100	0.41	100	1.7	25.1	8.6
253	0.78	100	0.27	100	0.16	100	7.45	0	45.2
393	0.94	82.5	0.4	100	0.2	100	8.67	0	96.5
433	1.08	21.5	0.67	100	0.11	100	5.9	0	15.2
654	1.14	7.45	0.35	100	0.29	100	1.21	16.2	43.7
1620	1.24	0.17	0.83	98.8	1.6	0	165.2	0	494.8
1685	0.97	65.2	0.57	100	0.34	100	7.96	0	15.2
2062	1.18	1.9	1	52.3	0.52	100	4.52	0	1.39
2063	0.78	93.1	0.88	78.3	1.18	18.7	15.1	0	5.7
2100	1.38	0.17	0.59	100	3.83	0	60.7	0	50.3
3103	0.88	92.3	1.01	45.7	0.24	100	0.33	82.1	0.34
3200	1.14	2.11	0.44	100	4.04	0	132.8	0	96.3
4183	1.04	28.1	0.52	100	0.24	100	0.02	99.1	0.01
4769	4.28	0	0.93	86.5	10	0	162.2	0	148.9
7889	1.04	36.2	0.58	100	0.02	100	0.39	89.8	0.2
10115	0.93	83.9	1.03	35.3	0.35	100	0.24	100	0.32
11066	0.95	79.4	0.64	100	0.67	99.9	3.32	0	1.14
16834	0.98	56	0.63	100	0.18	100	0.03	98.6	0.03
66391	13.12	0	2.44	0	51.5	0	79.3	0	8.9
68216	1.44	0.23	0.63	99.7	0.23	100	0.48	96.1	0.21
68950	1.26	0.79	1.01	44.3	3.8	0	29.9	0	16.2

5 Improving the procedure of the asteroid orbit determination

5.1 Modification in the dynamical modeling: Increase of the number of massive perturbers

In INPOP19a, the number of massive asteroids taken into account during the orbital integration is 353 for the planets and 16 for the asteroids. Beyond the comparison with Gaia Collaboration et al (2018b) where only 16 perturbers were included in the orbital computation, this difference in the dynamical modeling can also be explained by practical reasons. For a system of n objects with p perturbers, the total number of interactions $T(n, p)$ to account for is:

$$T(n, p) = (n - p) \times p + p \times (p - 1)/2 \quad (21)$$

Approximately, from Eq. 21, one can say that, considering the 14099 perturbed objects of Gaia DR2, the increase of the number of massive perturbers from 16 to 353 multiplies the number of interactions by a factor of 20. As each iteration takes 15 hours, the computational time for one iteration passes roughly from half a day to more than a week. Nevertheless, it is clear that the accuracy and the predictive capability of our trajectories will increase with the number of perturbers accounted for in the dynamical model. The goodness of the orbital adjustment on both Gaia

Table 8 Gaia post-fit residuals in case of an adjustment on both Gaia and radar, using a dynamical model including 353 perturbers and a weighting schema based on random error only.

properties: Asteroid:	residuals:								
	Gaia						Radar		
	AL		AC		Systematic		One-way		
	SER -	SVR %	SER -	SVR %	SER -	SVR %	SER -	SVR %	RMSE km
53	0.98	64.6	0.71	100	0.22	100	3.23	2.94	32.66
105	0.94	82	0.51	100	0.18	100	2.35	2.15	41.12
216	0.87	98.9	0.39	100	0.42	100	2.7	6.79	13.7
253	0.78	100	0.27	100	0.17	100	8.1	0	48.9
393	0.94	82.5	0.4	100	0.2	100	5.98	0	66.6
433	1.08	21.5	0.67	100	0.11	100	4.7	0	12.1
654	1.14	7.45	0.35	100	0.27	100	0.99	51.1	37.9
1620	1.23	0.23	0.83	98.6	0.39	100	1.17	35.8	1.93
1685	0.97	65.2	0.57	100	0.31	100	3.37	0	4.59
2062	1.18	2.02	1	47.6	0.45	100	1.35	16.2	0.39
2063	0.67	99	0.92	70.5	0.27	100	0.85	71.2	0.38
2100	1.01	46.4	0.54	100	0.24	100	0.75	84.1	0.58
3103	0.88	92.6	1.01	45.7	0.26	100	0.48	74.4	0.49
3200	1.08	12.5	0.45	100	0.3	100	5.02	0	4.23
4183	1.04	28.4	0.52	100	0.23	100	0.03	98.6	0.01
4769	1.03	29.9	0.94	80.4	0.34	100	2.1	0	1.66
7889	1.04	36.2	0.58	100	0.02	100	0.21	97.1	0.1
10115	0.93	83.5	1.04	30.1	0.35	100	0.23	100	0.28
11066	0.94	83.2	0.65	100	0.26	100	0.47	94.6	0.16
16834	0.98	56	0.63	100	0.17	100	0.03	98.6	0.03
66391	0.86	83.5	0.5	100	0.97	55.7	2.16	0	0.2
68216	1.44	0.23	0.65	99.5	0.13	100	0.54	93.8	0.27
68950	0.94	71.5	1.02	42.9	0.41	100	2.15	0	1.21

and radar observations is expected to follow the same trend. We thus perform a new orbital adjustment for the 23 selected objects (for which the computational time remains reasonable) using the same dynamical model as the one used for planets (353 massive perturbers). The asteroid masses are kept fixed and are not fitted in the present work. For a sake of comparison, we maintain the same weighting schema and adjustment procedure as the ones used in the previous section.

The statistics of post-fit residuals after the adjustment on both radar and Gaia observations are presented in Table 8. Compared to the orbits obtained with 16 perturbers, a clear improvement of the residuals is visible with only 8 objects with a SVR equals to zero (all on the radar residuals). 13 objects use to have SVRs equal to 0 in the previous case. (2063), (2100) and (11066) exhibit acceptable SVR values ($>70\%$ on both Gaia and radar) while they were rejected with the previous dynamical model (with radar SVR equals to 0%). (1620) and (2062) still have a small Gaia AL SVR of 0.23% and 2.02% respectively, but similar to the ones obtained with the solution fitted only on Gaia (Table 6) and with a radar SVR $>15\%$. The strong impact of the new dynamical model is also visible when comparing the radar statistics with the ones of Table 7. For 19 out of 23 objects, the increase of the number of perturbers from 16 to 353 leads to a significant reduction of the radar residuals, even when the SVR is still zero. For (3200), the improvement also includes the Gaia residuals with a SVR of 12.5% in AL, 100%

in AC and 100% for the systematic bias (respectively 7.1%, 100% and 0% in Table 6) and confirms that the badness of the adjustment of (3200) on Gaia only (Table 6) was caused by a lack in our previous dynamical model.

Another interesting point is to notice that for all the rejected combinations, the rejection criteria is exclusively encountered for the radar residuals as, in the same time, the Gaia ones remain acceptable. This behavior could be typically the sign of an over-weighting of the Gaia observations. In the next section, we study the impact of such an hypothesis by changing the weighting schema of our adjustment in order to take into account the impact of Gaia systematic errors during the fit .

5.2 Modification in the weighting schema: Introduction of the systematic errors

In Sect. 4.1, we proposed a method to compute the values of the Gaia systematic bias based on the minimization of the squared function (see Eq. 11). However, as the systematic bias was evaluated during the post-fit analysis, the asteroid initial conditions were adjusted on the basis of the squared function of Eq. 1, using a weight matrix that only accounts for random errors. It is then clear that the asteroid initial conditions were not optimized for the point of view of Eq. 11. In particular, Eq. 1 sees any increment of the systematic bias at the transit level as an increment of the estimated random errors of all the observations in the transit. As a consequence, the weighting schema is skewed leading to an over-constraint on the Gaia systematic bias, visible in Table 8 where the trade-off between Gaia and radar residuals always favours the Gaia observations.

There are two methods, mathematically equivalent, to fully account for both the systematic and the random errors in the fit . The first one consists in adding into the initial covariance matrix the Gaia systematic errors in quadratic with the random one , and then to use this new matrix as the inverse of the weight matrix W_{Gaia} (see Barlow (2021)), so that Eq. 1 could be rewritten as:

$$S = \xi_{Gaia}^T [W_{random+systematic}] \cdot \xi_{Gaia} \quad (22)$$

Eq. 22 is possible because the random and the systematic errors are independent so that one can add their variances. In practice, the 2x2 systematic covariance matrix provided by the DPAC for a transit with m observations, has to be extended to a $m \times m$ covariance matrix before its addition to the random error covariance matrix. If we call σ_{α_s} , σ_{δ_s} and cov_s , the systematic standard errors and the systematic covariance between α and δ for a given transit, the $m \times m$ systematic covariance matrix accounting for all the observations of the transit will be:

$$COV_{sys} = \begin{bmatrix} \sigma_{\alpha_s}^2 & cov_s & \sigma_{\alpha_s}^2 & cov_s & \sigma_{\alpha_s}^2 & \dots \\ cov_s & \sigma_{\delta_s}^2 & cov_s & \sigma_{\delta_s}^2 & cov_s & \dots \\ \sigma_{\alpha_s}^2 & cov_s & \sigma_{\alpha_s}^2 & cov_s & \sigma_{\alpha_s}^2 & \dots \\ cov_s & \sigma_{\delta_s}^2 & cov_s & \sigma_{\delta_s}^2 & cov_s & \dots \\ \sigma_{\alpha_s}^2 & cov_s & \sigma_{\alpha_s}^2 & cov_s & \sigma_{\alpha_s}^2 & \dots \\ \vdots & \vdots & \vdots & \vdots & \vdots & \ddots \end{bmatrix} \quad (23)$$

The presence of non-diagonal terms guarantees that a correlation equal to one is expected - from the point of view of the systematic - between each observation of the same transit, as they are impacted by the same systematic error.

One of the minor disadvantage of this method, based on the minimization of Eq 22, is that it doesn't directly provide the value of the obtained systematic bias, which still has to be computed following the procedure described in Sect. 4. Another method, mathematically similar (Barlow, 2021), consists in introducing the systematic bias as additional parameters in the fitting procedure and to directly minimize Eq. 11, in order to properly optimize the so-called bias-variance tradeoff. In the case where radar measurements are also included in the adjustment, Eq 11 must be rewritten as:

$$S = \sum_{i=1}^n \sum_{j=1}^{m_i} (\xi_{ij} - \beta_i)^T W_{ij} (\xi_{ij} - \beta_i) + \sum_{i=1}^n \beta_i^T V_i \beta_i + \xi_{radar}^T W_{radar} \xi_{radar} \quad (24)$$

The goal of the new least-square problem is now to minimize Eq 24. The adjusted parameters are the asteroid initial conditions and the vector β of the Gaia systematic bias, which are also included into the complete residuals:

$$\xi = \begin{bmatrix} \epsilon_{Gaia} \\ \beta_{sys} \\ \xi_{radar} \end{bmatrix} \quad (25)$$

ϵ_{Gaia} is the vector of the debiased residuals ($\xi_{ij} - \beta_i$) presented in Eq. 24, β_{sys} is the vector of the estimated bias and ξ_{radar} the radar residuals. The weight matrix becomes:

$$W = \begin{bmatrix} W_{random} & 0 & 0 \\ 0 & W_{sys} & 0 \\ 0 & 0 & W_{radar} \end{bmatrix} \quad (26)$$

and the Jacobian J:

$$J = \begin{bmatrix} J_{Gaia} & J_{sys} \\ 0 & \mathbb{1} \\ J_{radar} & 0 \end{bmatrix} \quad (27)$$

where $\mathbb{1}$ being the unit matrix and J_{sys} is the matrix of the derivative of ϵ_{gaia} with respect to β such as, for each element ij :

$$J_{sys}(ij) = \frac{\partial \epsilon_i}{\partial \beta_j} = \begin{cases} 1 & \text{if the observation } i \text{ belongs to the transit } j \\ 0 & \text{otherwise} \end{cases} \quad (28)$$

Substituting Eq. 26, 27, 25 into Eq. 2, we perform a new orbital adjustment of the orbits of the 23 selected objects using both Gaia and radar measurements, and the same list of 353 perturbers as in Sect. 5.1. The result of the post-fit analysis is presented on Table 9. We obtain acceptable SVRs for all the 23 studied objects confirming that the change in the weighting schema combined with a more complete dynamical model allows the orbital adjustment on both Gaia and radar with INPOP19a.

Two concerns can raise about the values obtained on Table 9. First, the small AL SVR (0.24 %, 2.04 % and 0.23 % respectively) obtained for (1620), (2062) and

Table 9 Gaia post-fit residuals in case of an adjustment on both Gaia and radar, using a dynamical model including 353 perturbers and a weighting schema based on both systematic and random error.

properties: Asteroid:	residuals:								
	Gaia						Radar		
	AL		AC		Systematic		One-way		
	SER -	SVR %	SER -	SVR %	SER -	SVR %	SER -	SVR %	RMSE km
53	0.98	64.6	0.71	100	0.22	100	0.01	99.7	0.06
105	0.94	82	0.52	100	0.18	100	0.78	65.9	13.6
216	0.87	98.9	0.39	100	0.41	100	0	99.8	0.02
253	0.78	100	0.27	100	0.17	100	0.01	99.3	0.08
393	0.94	82.5	0.4	100	0.19	100	0.02	99.1	0.18
433	1.08	21.5	0.67	100	0.17	100	0.02	100	0.06
654	1.14	7.45	0.35	100	0.26	100	0.36	100	20.9
1620	1.23	0.24	0.83	98.8	0.37	100	0.63	81.3	1.74
1685	0.97	65.5	0.57	100	0.4	100	0.27	100	0.4
2062	1.18	2.04	1	48.2	0.46	100	0.16	100	0.08
2063	0.67	99	0.93	70	0.38	100	0.44	99	0.32
2100	1.01	45.9	0.55	100	0.33	100	0.61	95.1	0.45
3103	0.87	93	1.01	45	0.23	100	0.02	98.9	0.02
3200	1.08	12.5	0.45	100	0.56	100	0.43	99.4	0.79
4183	1.04	28.7	0.52	100	0.2	100	0	100	0
4769	1.03	30.9	0.95	79.9	0.53	100	0.73	86.9	0.48
7889	1.04	36.2	0.56	100	0.15	100	0.19	97.6	0.09
10115	0.93	83.8	1.04	29.9	0.35	100	0.23	100	0.28
11066	0.94	83.8	0.65	100	0.23	100	0.25	99.5	0.08
16834	0.98	56.3	0.62	100	0.19	100	0	100	0
66391	0.89	78.3	0.49	100	1.48	1.02	0.45	100	0.09
68216	1.44	0.23	0.65	99.5	0.14	100	0.51	95.1	0.26
68950	0.95	69	1.02	43	0.68	99.2	1.01	47.3	0.51

(68216) appear to be suspicious. However, these values remain constant irrespective of the number of perturbers or the introduction of the systematic errors. This could mean that the misfit is more due to the data themselves than from the dynamical model or the fit. The second remark stands for (66391) - a binary NEA - for which the systematic SVR is only 1.02 %, contrasting with values greater than 99 % obtained for all the others objects. Comparing Table 7 and Table 8, we note that the residuals of (66391) are very sensitive to the change in the dynamical model, including GR (Verma et al (2017)). We cannot then exclude that its relative misfit could be still caused by a lack from this side. In particular, (66391) is known for being a candidate to Yarkosvsky effect detection (Vokrouhlický et al, 2000; Greenberg et al, 2020). Adding such a non-gravitational perturbation in our dynamical model is behind the scope of this paper but could be an interesting possibility in the perspective of Gaia DR3. In the case of (1620) and (2062), we note that our modeling did not include Doppler measurements that have been obtained together with or even before the range data. These Doppler observations are crucial for poorly constrained objects as they give an accurate estimation of the asteroid radial velocity which is an important parameter especially for very fast objects. For (1620), they were even more Doppler measurements than range observations. For (2062) there are more range observations (6 against 2 Doppler) but the first Doppler observation was obtained 17 years before the range session,

increasing the time interval of the fit and consequently the time resolution of the adjustment. A next future improvement will be to include the Doppler observations to our analysis.

6 Conclusion and perspective

We perform the orbital determination of 14099 asteroids for which observations have been delivered on the Gaia DR2, gathering nearly 2 millions of observations, using INPOP19a planetary ephemerides and a dynamical modeling similar to Gaia Collaboration et al (2018b). Two new aspects were investigated :

- we point out the fact that because of the SSB shift between INPOP10e and INPOP19a due to the addition of ten massive TNOs, the barycentric positions of the Gaia satellite provided by DR2 at J2000 cannot be directly used. Assuming that the geocentric state is obtained with ground-based tracking data, we then consider the Earth-spacecraft vector that we shift from INPOP10e to INPOP19a in order to deduce the Gaia positions into the INPOP19a frame. However, to avoid a systematic comparison with INPOP10e when using another ephemerides, we recommend to provide for the future Gaia releases, the Gaia satellite positions in a minimal model-dependent parametrization .
- we develop a convenient mathematical formalism for the resolution of the least-square problem, according for perturbers influences on the perturbed orbits. This formalism will be very useful in the perspective of Gaia DR3 as it presents two advantages: it is capable of handling small matrices independently from the number of observations. It includes also global parameters such as object masses. The estimation of global parameters is not possible if one adjusts the orbits as if they were independent. By introducing such formalism we prepare the venue of the Gaia DR3 and the determination of masses together with the orbit adjustment.

As a result and considering only Gaia observations, we obtain Gaia post-fit residuals in good accordance with Gaia Collaboration et al (2018b), confirming the magnitude dependency and the milliarcsecond accuracy level in the AL direction. We also perform a careful post-fit analysis, including the effect of the Gaia systematic errors, for a selection of 23 objects, inferring a good accordance between the obtained residuals and the expected error model announced by Gaia-DR2. However, as the Gaia-DR2 time coverage is only 22 months, we also perform a global orbit adjustment using both Gaia and radar measurements in order to check the validity of the obtained trajectories and the compatibility of Gaia-DR2 with other datasets. Using 16 perturbers and a weighting schema only based on random errors, we were unable to find a good fit in combining both Gaia and radar observations as 13 objects over the mentioned 23 remain with χ^2 greater than expected. We identified several improvements that must be carried to the procedure described by Gaia Collaboration et al (2018b) when combining Gaia angular observations with radar distances:

- The inclusion of the radar measurements is incomplete in our present work. We account for the range observations but not the Doppler measurements. These type of measurements are rare but can be very useful when very few range observation are available or when the addition of Doppler measurements can

help for increasing the time span of the observational data sets as it was the case for (1620) and (2062).

- Addition of MPC observations. In some cases, the prolongation of the time span of the observational data sets can help for improving the quality of the fit and to test the consistency of the present orbits. This next step will be investigated.
- An improvement of the dynamical model. The number of perturbers was increased from 16 to 353 in order to ensure the accuracy of the adjusted orbits over an interval longer than the Gaia-DR2 time coverage.
- An improvement of the weighting schema. The Gaia systematic errors must be taken into account during the adjustment and not only during the post-fit analysis. This could be done by adding the systematic covariance to the random one when computing the inverse of the weight matrix, or by adding the systematic bias as an explicit parameter to be adjusted during the fit. General Relativity will be also included into the asteroid dynamical model.

Finally, one can expect great perspectives for the future Gaia DR3, in particular concerning mass determinations, the introduction of the Yarkovsky effect in our dynamical model and tests of General Relativity with a full consistent planetary and asteroid orbits.

Acknowledgement

The authors would like to thank the reviewers for their constructive and helpful remarks, in particular concerning the use of the Gaia systematic error during the post fit analysis and the weighting procedure.

References

- Barlow, R.: Combining experiments with systematic errors. *Nuclear Instruments and Methods in Physics Research Section A: Accelerators, Spectrometers, Detectors and Associated Equipment* **987**, 164,864 (2021)
- Carpino, M., Milani, A., Chesley, S.R.: Error statistics of asteroid optical astrometric observations. *Icarus* **166**(2), 248 – 270 (2003)
- Chesley, S.R., Baer, J., Monet, D.G.: Treatment of star catalog biases in asteroid astrometric observations. *Icarus* **210**(1), 158–181 (2010)
- Di Ruscio, A., Fienga, A., Durante, D., Iess, L., Laskar, J., Gastineau, M.: Analysis of Cassini radio tracking data for the construction of INPOP19a: A new estimate of the Kuiper belt mass. *A&A* **640**:A7 (2020a)
- Di Ruscio, A., Fienga, A., Durante, D., Iess, L., Laskar, J. and Gastineau, M.: An estimate of the Kuiper belt mass from Cassini tracking data and INPOP19a. *A&A* (in press) (2020b)
- Farnocchia, D., Chesley, S.R., Chamberlin, A.B., Tholen, D.J.: Star catalog position and proper motion corrections in asteroid astrometry. *Icarus* **245**, 94–111 (2015)
- Fienga, A., Manche, H., Laskar, J., Gastineau, M.: INPOP06, a new numerical ephemeris. In: Capitaine, N. (ed) *Journées Systèmes de Référence Spatio-temporels 2007*, p 69 (2008a)

- Fienga, A., Manche, H., Laskar, J., Gastineau, M.: INPOP06: a new numerical planetary ephemeris. *A&A* **477**, 315–327 (2008b)
- Fienga, A., Laskar, J., Morley, T., Manche, H., Kuchynka, P., Le Poncin-Lafitte, C., Budnik, F., Gastineau, M., Somenzi, L.: INPOP08, a 4-D planetary ephemeris: from asteroid and time-scale computations to ESA Mars Express and Venus Express contributions. *A&A* **507**, 1675–1686 (2009)
- Fienga, A., Laskar, J., Kuchynka, P., Manche, H., Desvignes, G., Gastineau, M., Cognard, I., Theureau, G.: The INPOP10a planetary ephemeris and its applications in fundamental physics. *Celestial Mechanics and Dynamical Astronomy* **111**, 363–385 (2011a)
- Fienga, A., Laskar, J., Kuchynka, P., Manche, H., Desvignes, G., Gastineau, M., Cognard, I., Theureau, G.: The INPOP10a planetary ephemeris and its applications in fundamental physics. *Celestial Mechanics and Dynamical Astronomy* **111**(3), 363–385 (2011b)
- Fienga, A., Laskar, J., Manche, H., Gastineau, M., Verma, A.: DPAC INPOP final release: INPOP10e. ArXiv e-prints (2012)
- Fienga, A., Manche, H., Laskar, J., Gastineau, M., Verma, A.: INPOP new release: INPOP10e. arXiv e-prints arXiv:1301.1510 (2013)
- Fienga, A., Laskar, J., Manche, H., Gastineau, M., Verma, A.: New inpop release: Inpop13c. ArXiv e-prints (2014)
- Fienga, A., Laskar, J., Exertier, P., Manche, H., Gastineau, M.: Numerical estimation of the sensitivity of INPOP planetary ephemerides to general relativity parameters. *Celestial Mechanics and Dynamical Astronomy* **123**, 325–349 (2015a)
- Fienga, A., Laskar, J., Exertier, P., Manche, H., Gastineau, M.: Numerical estimation of the sensitivity of INPOP planetary ephemerides to general relativity parameters. *Celestial Mechanics and Dynamical Astronomy* **123**, 325–349 (2015b)
- Fienga, A., Manche, H., Laskar, J., Gastineau, M., Verma, A.: GAIA DPAC INPOP final release: INPOP10e. *Notes Scientifiques et Techniques de l’Institut de Mecanique Celeste* **104** (2016)
- Fienga, A., Avdellidou, C., Hanuš, J.: Asteroid masses obtained with INPOP planetary ephemerides. *MNRAS* p 3035 (2019a)
- Fienga, A., Deram, P., Viswanathan, V., Di Ruscio, A., Bernus, L., Durante, D., Gastineau, M., Laskar, J.: INPOP19a planetary ephemerides. *Notes Scientifiques et Techniques de l’Institut de Mecanique Celeste* **109** (2019b)
- Fienga, A., Deram, P., Viswanathan, V., Di Ruscio, A., Bernus, L., Durante, D., Gastineau, M., Laskar, J.: INPOP19a planetary ephemeris. *Notes Scientifiques et Techniques de l’Institut de Mecanique Celeste* **109** (2019c)
- Folkner, W.: JPL Interoffice Memorandum IOM 343.R-10-001: Planetary ephemeris DE423 fit to Messenger encounters with Mercury. Tech. rep., JPL Interoffice Memorandum IOM 343.R-10-001 (2010)
- Folkner, W.M., Williams, J.G., Boggs, D.H., Park, R.S., Kuchynka, P.: The Planetary and Lunar Ephemerides DE430 and DE431. *Interplanetary Network Progress Report* **196**, C1 (2014)
- Gaia Collaboration, Prusti, T., de Bruijne, J.H.J., Brown, A.G.A., Vallenari, A., Babusiaux, C., Bailer-Jones, C.A.L., Bastian, U., Biermann, M., Evans, D.W., Eyer, L., Jansen, F., Jordi, C., Klioner, S.A., Lammers, U., Lindgren, L., Luri, X., Mignard, F., Milligan, D.J., Panem, C., Poinsignon, V., Pour-

baix, D., Randich, S., Sarri, G., Sartoretti, P., Siddiqui, H.I., Soubiran, C., Valette, V., van Leeuwen, F., Walton, N.A., Aerts, C., Arenou, F., Cropper, M., Drimmel, R., Høg, E., Katz, D., Lattanzi, M.G., O'Mullane, W., Grebel, E.K., Holland, A.D., Huc, C., Passot, X., Bramante, L., Cacciari, C., Castañeda, J., Chaoul, L., Cheek, N., De Angeli, F., Fabricius, C., Guerra, R., Hernández, J., Jean-Antoine-Piccolo, A., Masana, E., Messineo, R., Mowlavi, N., Nienartowicz, K., Ordóñez-Blanco, D., Panuzzo, P., Portell, J., Richards, P.J., Riello, M., Seabroke, G.M., Tanga, P., Thévenin, F., Torra, J., Els, S.G., Gracia-Abril, G., Comoretto, G., Garcia-Reinaldos, M., Lock, T., Mercier, E., Altmann, M., Andrae, R., Astraatmadja, T.L., Bellas-Velidis, I., Benson, K., Berthier, J., Blomme, R., Busso, G., Carry, B., Cellino, A., Clementini, G., Cowell, S., Creevey, O., Cuypers, J., Davidson, M., De Ridder, J., de Torres, A., Delchambre, L., Dell'Oro, A., Ducourant, C., Frémat, Y., García-Torres, M., Gosset, E., Halbwachs, J.L., Hambly, N.C., Harrison, D.L., Hauser, M., Hestroffer, D., Hodgkin, S.T., Huckle, H.E., Hutton, A., Jasniewicz, G., Jordan, S., Kontizas, M., Korn, A.J., Lanzafame, A.C., Manteiga, M., Moitinho, A., Muinonen, K., Osinde, J., Pancino, E., Pauwels, T., Petit, J.M., Recio-Blanco, A., Robin, A.C., Sarro, L.M., Siopis, C., Smith, M., Smith, K.W., Sozzetti, A., Thuillot, W., van Reeve, W., Viala, Y., Abbas, U., Abreu Aramburu, A., Accart, S., Aguado, J.J., Allan, P.M., Allasia, W., Altavilla, G., Álvarez, M.A., Alves, J., Anderson, R.I., Andrei, A.H., Anglada Varela, E., Antiche, E., Antoja, T., Antón, S., Arcay, B., Atzei, A., Ayache, L., Bach, N., Baker, S.G., Balaguer-Núñez, L., Barache, C., Barata, C., Barbier, A., Barblan, F., Baroni, M., Barrado y Navascués, D., Barros, M., Barstow, M.A., Becciani, U., Bellazzini, M., Bellei, G., Bello García, A., Belokurov, V., Bendjoya, P., Berihuete, A., Bianchi, L., Bienaymé, O., Billebaud, F., Blagorodnova, N., Blanco-Cuaresma, S., Boch, T., Bombrun, A., Borrachero, R., Bouquillon, S., Bourda, G., Bouy, H., Bragaglia, A., Breddels, M.A., Brouillet, N., Brüsemeister, T., Bucciarelli, B., Budnik, F., Burgess, P., Burgon, R., Burlacu, A., Busonero, D., Buzzzi, R., Caffau, E., Cambras, J., Campbell, H., Cancelliere, R., Cantat-Gaudin, T., Carlucci, T., Carrasco, J.M., Castellani, M., Charlot, P., Charnas, J., Charvet, P., Chassat, F., Chiavassa, A., Clotet, M., Cocozza, G., Collins, R.S., Collins, P., Costigan, G., Crifo, F., Cross, N.J.G., Crosta, M., Crowley, C., Dafonte, C., Damerjji, Y., Dapergolas, A., David, P., David, M., De Cat, P., de Felice, F., de Laverny, P., De Luise, F., De March, R., de Martino, D., de Souza, R., Debosscher, J., del Pozo, E., Delbo, M., Delgado, A., Delgado, H.E., di Marco, F., Di Matteo, P., Diakite, S., Distefano, E., Dolding, C., Dos Anjos, S., Drazinos, P., Durán, J., Dzigan, Y., Ecale, E., Edvardsson, B., Enke, H., Erdmann, M., Escolar, D., Espina, M., Evans, N.W., Eynard Bontemps, G., Fabre, C., Fabrizio, M., Faigler, S., Falcão, A.J., Farràs Casas, M., Faye, F., Federici, L., Fedorets, G., Fernández-Hernández, J., Fernique, P., Fienga, A., Figueras, F., Filippi, F., Findeisen, K., Fonti, A., Fouesneau, M., Fraile, E., Fraser, M., Fuchs, J., Furnell, R., Gai, M., Galletti, S., Galluccio, L., Garabato, D., García-Sedano, F., Garé, P., Garofalo, A., Garralda, N., Gavras, P., Gerssen, J., Geyer, R., Gilmore, G., Girona, S., Giuffrida, G., Gomes, M., González-Marcos, A., González-Núñez, J., González-Vidal, J.J., Granvik, M., Guerrier, A., Guillout, P., Guiraud, J., Gúrpide, A., Gutiérrez-Sánchez, R., Guy, L.P., Haignon, R., Hatidimitriou, D., Haywood, M., Heiter, U., Helmi, A., Hobbs, D., Hofmann, W., Holl, B., Holland, G., Hunt, J.A.S., Hypki, A., Icardi, V., Irwin, M., Jevardat de Fombelle, G.,

Jofré, P., Jonker, P.G., Jorissen, A., Julbe, F., Karampelas, A., Kochoska, A., Kohley, R., Kolenberg, K., Kontizas, E., Kuposov, S.E., Kordopatis, G., Koub-sky, P., Kowalczyk, A., Krone-Martins, A., Kudryashova, M., Kull, I., Bachchan, R.K., Lacoste-Seris, F., Lanza, A.F., Lavigne, J.B., Le Poncin-Lafitte, C., Le-breton, Y., Lebzelter, T., Leccia, S., Leclerc, N., Lecoeur-Taïbi, I., Lemaitre, V., Lenhardt, H., Leroux, F., Liao, S., Licata, E., Lindstrøm, H.E.P., Lister, T.A., Livanou, E., Lobel, A., Löffler, W., López, M., Lopez-Lozano, A., Lorenz, D., Loureiro, T., MacDonald, I., Magalhães Fernandes, T., Managau, S., Mann, R.G., Mantelet, G., Marchal, O., Marchant, J.M., Marconi, M., Marie, J., Mari-noni, S., Marrese, P.M., Marschalkó, G., Marshall, D.J., Martín-Fleitas, J.M., Martino, M., Mary, N., Matijevič, G., Mazeh, T., McMillan, P.J., Messina, S., Mestre, A., Michalik, D., Millar, N.R., Miranda, B.M.H., Molina, D., Molinaro, R., Molinaro, M., Molnár, L., Moniez, M., Montegriffo, P., Monteiro, D., Mor, R., Mora, A., Morbidelli, R., Morel, T., Morgenthaler, S., Morley, T., Mor-ris, D., Mulone, A.F., Muraveva, T., Musella, I., Narbonne, J., Nelemans, G., Nicastro, L., Noval, L., Ordénovic, C., Ordieres-Meré, J., Osborne, P., Pagani, C., Pagano, I., Pailler, F., Palacin, H., Palaversa, L., Parsons, P., Paulsen, T., Pecoraro, M., Pedrosa, R., Pentikäinen, H., Pereira, J., Pichon, B., Piersimoni, A.M., Pineau, F.X., Plachy, E., Plum, G., Poujoulet, E., Prša, A., Pulone, L., Ragaini, S., Rago, S., Rambaux, N., Ramos-Lerate, M., Ranalli, P., Rauw, G., Read, A., Regibo, S., Renk, F., Reyly, C., Ribeiro, R.A., Rimoldini, L., Ripepi, V., Riva, A., Rixon, G., Roelens, M., Romero-Gómez, M., Rowell, N., Royer, F., Rudolph, A., Ruiz-Dern, L., Sadowski, G., Sagristà Sellés, T., Sahlmann, J., Salgado, J., Salguero, E., Sarasso, M., Savietto, H., Schnorhk, A., Schultheis, M., Sciacca, E., Segol, M., Segovia, J.C., Segransan, D., Serpell, E., Shih, I.C., Smareglia, R., Smart, R.L., Smith, C., Solano, E., Solitro, F., Sordo, R., Soria Nieto, S., Souchay, J., Spagna, A., Spoto, F., Stampa, U., Steele, I.A., Stei-delmüller, H., Stephenson, C.A., Stoev, H., Suess, F.F., Süveges, M., Surdej, J., Szabados, L., Szegedi-Elek, E., Tapiador, D., Taris, F., Tauran, G., Taylor, M.B., Teixeira, R., Terrett, D., Tingley, B., Trager, S.C., Turon, C., Ulla, A., Utrilla, E., Valentini, G., van Elteren, A., Van Hemelryck, E., van Leeuwen, M., Varadi, M., Vecchiato, A., Veljanoski, J., Via, T., Vicente, D., Vogt, S., Voss, H., Votruba, V., Voutsinas, S., Walmsley, G., Weiler, M., Weingrill, K., Werner, D., Wevers, T., Whitehead, G., Wyrzykowski, L., Yoldas, A., Žerjal, M., Zucker, S., Zurbach, C., Zwitter, T., Alecu, A., Allen, M., Allende Prieto, C., Amorim, A., Anglada-Escudé, G., Arsenijevic, V., Azaz, S., Balm, P., Beck, M., Bernstein, H.H., Bigot, L., Bijaoui, A., Blasco, C., Bonfigli, M., Bono, G., Boudreault, S., Bressan, A., Brown, S., Brunet, P.M., Bunclark, P., Buonanno, R., Butkevich, A.G., Carret, C., Carrion, C., Chemin, L., Chéreau, F., Corcione, L., Darmigny, E., de Boer, K.S., de Teodoro, P., de Zeeuw, P.T., Delle Luche, C., Domingues, C.D., Dubath, P., Fodor, F., Frézouls, B., Fries, A., Fustes, D., Fyfe, D., Gallardo, E., Gallegos, J., Gardiol, D., Gebran, M., Gomboc, A., Gómez, A., Grux, E., Gueguen, A., Heyrovsky, A., Hoar, J., Iannicola, G., Isasi Parache, Y., Janotto, A.M., Joliet, E., Jonckheere, A., Keil, R., Kim, D.W., Klagyivik, P., Klar, J., Knude, J., Kochukhov, O., Kolka, I., Kos, J., Kutka, A., Lainey, V., LeBouquin, D., Liu, C., Loreggia, D., Makarov, V.V., Marseille, M.G., Martayan, C., Martinez-Rubi, O., Massart, B., Meynadier, F., Mignot, S., Munari, U., Nguyen, A.T., Nordlander, T., Ocvirk, P., O’Flaherty, K.S., Olias Sanz, A., Ortiz, P., Osorio, J., Oszkiewicz, D., Ouzounis, A., Palmer, M., Park,

P., Pasquato, E., Peltzer, C., Peralta, J., Péturaud, F., Pieniluoma, T., Pigozzi, E., Poels, J., Prat, G., Prod'homme, T., Raison, F., Rebordao, J.M., Risquez, D., Rocca-Volmerange, B., Rosen, S., Ruiz-Fuertes, M.I., Russo, F., Sembay, S., Serraller Vizcaino, I., Short, A., Siebert, A., Silva, H., Sinachopoulos, D., Slezak, E., Soffel, M., Sosnowska, D., Straizys, V., ter Linden, M., Terrell, D., Theil, S., Tiede, C., Troisi, L., Tsalmantza, P., Tur, D., Vaccari, M., Vachier, F., Valles, P., Van Hamme, W., Veltz, L., Virtanen, J., Wallut, J.M., Wichmann, R., Wilkinson, M.I., Ziaepour, H., Zschocke, S.: The Gaia mission. *A&A* **595**:A1 (2016)

Gaia Collaboration, Mignard, F., Klioner, S. A., Lindegren, L., Hernández, J., Bastian, U., Bombrun, A., Hobbs, D., Lammers, U., Michalik, D., Ramos-Lerate, M., Biermann, M., Fernández-Hernández, J., Geyer, R., Hilger, T., Siddiqui, H. I., Steidelmüller, H., Babusiaux, C., Barache, C., Lambert, S., Andrei, A. H., Bourda, G., Charlot, P., Brown, A. G. A., Vallenari, A., Prusti, T., de Bruijne, J. H. J., Bailer-Jones, C. A. L., Evans, D. W., Eyer, L., Jansen, F., Jordi, C., Luri, X., Panem, C., Pourbaix, D., Randich, S., Sartoretti, P., Soubiran, C., van Leeuwen, F., Walton, N. A., Arenou, F., Cropper, M., Drimmel, R., Katz, D., Lattanzi, M. G., Bakker, J., Cacciari, C., Castañeda, J., Chaoul, L., Cheek, N., De Angeli, F., Fabricius, C., Guerra, R., Holl, B., Masana, E., Messineo, R., Mowlavi, N., Nienartowicz, K., Panuzzo, P., Portell, J., Riello, M., Seabroke, G. M., Tanga, P., Thévenin, F., Gracia-Abril, G., Comoretto, G., Garcia-Reinaldos, M., Teyssier, D., Altmann, M., Andrae, R., Audard, M., Bellas-Velidis, I., Benson, K., Berthier, J., Blomme, R., Burgess, P., Busso, G., Carry, B., Cellino, A., Clementini, G., Clotet, M., Creevey, O., Davidson, M., De Ridder, J., Delchambre, L., Dell'Oro, A., Ducourant, C., Fouesneau, M., Frémat, Y., Galluccio, L., García-Torres, M., González-Núñez, J., González-Vidal, J. J., Gosset, E., Guy, L. P., Halbwegs, J.-L., Hambly, N. C., Harrison, D. L., Hestroffer, D., Hodgkin, S. T., Hutton, A., Jasiewicz, G., Jean-Antoine-Piccolo, A., Jordan, S., Korn, A. J., Krone-Martins, A., Lanzafame, A. C., Lebzelter, T., Löffler, W., Manteiga, M., Marrese, P. M., Martín-Fleitas, J. M., Moitinho, A., Mora, A., Muinonen, K., Osinde, J., Pancino, E., Pauwels, T., Petit, J.-M., Recio-Blanco, A., Richards, P. J., Rimoldini, L., Robin, A. C., Sarro, L. M., Siopis, C., Smith, M., Sozzetti, A., Süveges, M., Torra, J., van Reeve, W., Abbas, U., Abreu Aramburu, A., Accart, S., Aerts, C., Altavilla, G., Álvarez, M. A., Alvarez, R., Alves, J., Anderson, R. I., Anglada Varela, E., Antiche, E., Antoja, T., Arcay, B., Astraatmadja, T. L., Bach, N., Baker, S. G., Balaguer-Núñez, L., Balm, P., Barata, C., Barbato, D., Barblan, F., Barklem, P. S., Barrado, D., Barros, M., Barstow, M. A., Bartholomé Muñoz, L., Bassilana, J.-L., Becciani, U., Bellazzini, M., Berihuete, A., Bertone, S., Bianchi, L., Bienaymé, O., Blanco-Cuaresma, S., Boch, T., Boeche, C., Borrachero, R., Bossini, D., Bouquillon, S., Bragaglia, A., Bramante, L., Breddels, M. A., Bressan, A., Brouillet, N., Brüsmeister, T., Brugaletta, E., Bucciarelli, B., Burlacu, A., Busonero, D., Butkevich, A. G., Buzzi, R., Caffau, E., Cancelliere, R., Cannizzaro, G., Cantat-Gaudin, T., Carballo, R., Carlucci, T., Carrasco, J. M., Casamiquela, L., Castellani, M., Castro-Ginard, A., Chemin, L., Chiavassa, A., Cocozza, G., Costigan, G., Cowell, S., Crifo, F., Crosta, M., Crowley, C., Cuypers, J., Dafonte, C., Damerdj, Y., Dapergolas, A., David, P., David, M., de Laverny, P., De Luise, F., De March, R., de Souza, R., de Torres, A., Deboscher, J., del Pozo, E., Delbo, M., Delgado, A., Delgado, H. E., Diakite, S., Diener, C., Distefano, E., Dolding, C., Drazinos,

- P., Durán, J., Edvardsson, B., Enke, H., Eriksson, K., Esquej, P., Eynard Bon-temps, G., Fabre, C., Fabrizio, M., Faigler, S., Falcão, A. J., Farràs Casas, M., Federici, L., Fedorets, G., Fernique, P., Figueras, F., Filippi, F., Findeisen, K., Fonti, A., Fraile, E., Fraser, M., Frézouls, B., Gai, M., Galleti, S., Garabato, D., García-Sedano, F., Garofalo, A., Garralda, N., Gavel, A., Gavras, P., Gerssen, J., Giacobbe, P., Gilmore, G., Girona, S., Giuffrida, G., Glass, F., Gomes, M., Granvik, M., Gueguen, A., Guerrier, A., Guiraud, J., Gutiérrez, R., Haigron, R., Hatzidimitriou, D., Hauser, M., Haywood, M., Heiter, U., Helmi, A., Heu, J., Hofmann, W., Holland, G., Huckle, H. E., Hypki, A., Icardi, V., Janßen, K., Jevardat de Fombelle, G., Jonker, P. G., Juhász, A. L., Julbe, F., Karampelas, A., Kewley, A., Klar, J., Kochoska, A., Kohley, R., Kolenberg, K., Kontizas, M., Kontizas, E., Koposov, S. E., Kordopatis, G., Kostrzewa-Rutkowska, Z., Koub-sky, P., Lanza, A. F., Lasne, Y., Lavigne, J.-B., Le Fustec, Y., Le Poncin-Lafitte, C., Lebreton, Y., Leccia, S., Leclerc, N., Lecoeur-Taïbi, I., Lenhardt, H., Leroux, F., Liao, S., Licata, E., Lindstrøm, H. E. P., Lister, T. A., Livanou, E., Lobel, A., López, M., Managau, S., Mann, R. G., Mantelet, G., Marchal, O., Marchant, J. M., Marconi, M., Marinoni, S., Marschalkó, G., Marshall, D. J., Martino, M., Marton, G., Mary, N., Massari, D., Matijevic, G., Mazeh, T., McMillan, P. J., Messina, S., Millar, N. R., Molina, D., Molinaro, R., Molnár, L., Montegriffo, P., Mor, R., Morbidelli, R., Morel, T., Morris, D., Mulone, A. F., Muraveva, T., Musella, I., Nelemans, G., Nicastrò, L., Noval, L., O'Mullane, W., Ordénovic, C., Ordóñez-Blanco, D., Osborne, P., Pagani, C., Pagano, I., Pailler, F., Palacin, H., Palaversa, L., Panahi, A., Pawlak, M., Piersimoni, A. M., Pineau, F.-X., Plachy, E., Plum, G., Poggio, E., Poujoulet, E., Prsa, A., Pulone, L., Racero, E., Ragaini, S., Rambaux, N., Regibo, S., Reylé, C., Riclet, F., Ripepi, V., Riva, A., Rivard, A., Rixon, G., Roegiers, T., Roelens, M., Romero-Gómez, M., Row-ell, N., Royer, F., Ruiz-Dern, L., Sadowski, G., Sagristà Sellés, T., Sahlmann, J., Salgado, J., Salguero, E., Sanna, N., Santana-Ros, T., Sarasso, M., Savietto, H., Schultheis, M., Sciacca, E., Segol, M., Segovia, J. C., Ségransan, D., Shih, I.-C., Siltala, L., Silva, A. F., Smart, R. L., Smith, K. W., Solano, E., Solitro, F., Sordo, R., Soria Nieto, S., Souchay, J., Spagna, A., Spoto, F., Stampa, U., Steele, I. A., Stephenson, C. A., Stoev, H., Suess, F. F., Surdej, J., Szabados, L., Szegedi-Elek, E., Tapiador, D., Taris, F., Tauran, G., Taylor, M. B., Teixeira, R., Terrett, D., Teyssandier, P., Thuillot, W., Titarenko, A., Torra Clotet, F., Turon, C., Ulla, A., Utrilla, E., Uzzi, S., Vaillant, M., Valentini, G., Valette, V., van Elteren, A., Van Hemelryck, E., van Leeuwen, M., Vaschetto, M., Vecchi-ato, A., Veljanoski, J., Viala, Y., Vicente, D., Vogt, S., von Essen, C., Voss, H., Votruba, V., Voutsinas, S., Walmsley, G., Weiler, M., Wertz, O., Wevers, T., Wyrzykowski, L., Yoldas, A., Zerjal, M., Ziaepour, H., Zorec, J., Zschocke, S., Zucker, S., Zurbach, C., Zwitter, T.: Gaia data release 2 - the celestial reference frame (gaia-crfl2). *A&A* **616**, A14 (2018a)
- Gaia Collaboration, Spoto, F., Tanga, P., Mignard, F., Berthier, J., Carry, B., Cellino, A., Dell'Oro, A., Hestroffer, D., Muinonen, K., Pauwels, T., Petit, J.M., David, P., De Angeli, F., Delbo, M., Frézouls, B., Galluccio, L., Granvik, M., Guiraud, J., Hernández, J., Ordénovic, C., Portell, J., Poujoulet, E., Thuil-lot, W., Walmsley, G., Brown, A.G.A., Vallenari, A., Prusti, T., de Bruijne, J.H.J., Babusiaux, C., Bailer-Jones, C.A.L., Biermann, M., Evans, D.W., Eyer, L., Jansen, F., Jordi, C., Klioner, S.A., Lammers, U., Lindegren, L., Luri, X., Panem, C., Pourbaix, D., Randich, S., Sartoretti, P., Siddiqui, H.I., Soubiran,

C., van Leeuwen, F., Walton, N.A., Arenou, F., Bastian, U., Cropper, M., Drimmel, R., Katz, D., Lattanzi, M.G., Bakker, J., Cacciari, C., Castañeda, J., Chaoul, L., Cheek, N., Fabricius, C., Guerra, R., Holl, B., Masana, E., Messineo, R., Mowlavi, N., Nienartowicz, K., Panuzzo, P., Riello, M., Seabroke, G.M., Thévenin, F., Gracia-Abril, G., Comoretto, G., Garcia-Reinaldos, M., Teyssier, D., Altmann, M., Andrae, R., Audard, M., Bellas-Velidis, I., Benson, K., Blomme, R., Burgess, P., Busso, G., Clementini, G., Clotet, M., Creevey, O., Davidson, M., De Ridder, J., Delchambre, L., Ducourant, C., Fernández-Hernández, J., Fouesneau, M., Frémat, Y., García-Torres, M., González-Núñez, J., González-Vidal, J.J., Gosset, E., Guy, L.P., Halbwachs, J.L., Hambly, N.C., Harrison, D.L., Hodgkin, S.T., Hutton, A., Jasniewicz, G., Jean-Antoine-Piccolo, A., Jordan, S., Korn, A.J., Krone-Martins, A., Lanzafame, A.C., Lebzelter, T., Lö, W., Manteiga, M., Marrese, P.M., Martín-Fleitas, J.M., Moitinho, A., Mora, A., Osinde, J., Pancino, E., Recio-Blanco, A., Richards, P.J., Rimoldini, L., Robin, A.C., Sarro, L.M., Siopis, C., Smith, M., Sozzetti, A., Süveges, M., Torra, J., van Reeven, W., Abbas, U., Abreu Aramburu, A., Accart, S., Aerts, C., Altavilla, G., Álvarez, M.A., Alvarez, R., Alves, J., Anderson, R.I., Andrei, A.H., Anglada Varela, E., Antiche, E., Antoja, T., Arcay, B., Astraatmadja, T.L., Bach, N., Baker, S.G., Balaguer-Núñez, L., Balm, P., Barache, C., Barata, C., Barbato, D., Barblan, F., Barklem, P.S., Barrado, D., Barros, M., Barstow, M.A., Bartholomé Muñoz, L., Bassilana, J.L., Becciani, U., Bellazzini, M., Berihuete, A., Bertone, S., Bianchi, L., Bienaymé, O., Blanco-Cuaresma, S., Boch, T., Boeche, C., Bombrun, A., Borrachero, R., Bossini, D., Bouquillon, S., Bourda, G., Bragaglia, A., Bramante, L., Breddels, M.A., Bressan, A., Brouillet, N., Brüsemeister, T., Brugaletta, E., Bucciarelli, B., Burlacu, A., Busonero, D., Butkevich, A.G., Buzzi, R., Caffau, E., Cancelliere, R., Cannizzaro, G., Cantat-Gaudin, T., Carballo, R., Carlucci, T., Carrasco, J.M., Casamiquela, L., Castellani, M., Castro-Ginard, A., Charlot, P., Chemin, L., Chiavassa, A., Cocozza, G., Costigan, G., Cowell, S., Crifo, F., Crosta, M., Crowley, C., Cuypers, J., Dafonte, C., Damerджи, Y., Dapergolas, A., David, M., de Laverny, P., De Luise, F., De March, R., de Souza, R., de Torres, A., Debosscher, J., del Pozo, E., Delgado, A., Delgado, H.E., Diakite, S., Diener, C., Distefano, E., Dolding, C., Drazinos, P., Durán, J., Edvardsson, B., Enke, H., Eriksson, K., Esquej, P., Eynard Bontemps, G., Fabre, C., Fabrizio, M., Faigler, S., Falcão, A.J., Farràs Casas, M., Federici, L., Fedorets, G., Fernique, P., Figueras, F., Filippi, F., Findeisen, K., Fonti, A., Fraile, E., Fraser, M., Gai, M., Galleti, S., Garabato, D., García-Sedano, F., Garofalo, A., Garralda, N., Gavel, A., Gavras, P., Gerssen, J., Geyer, R., Giacobbe, P., Gilmore, G., Girona, S., Giuffrida, G., Glass, F., Gomes, M., Gueguen, A., Guerrier, A., Gutiérrez, R., Haigron, R., Hatzidimitriou, D., Hauser, M., Haywood, M., Heiter, U., Helmi, A., Heu, J., Hilger, T., Hobbs, D., Hofmann, W., Holland, G., Huckle, H.E., Hypki, A., Icardi, V., Janßen, K., Jevardat de Fombelle, G., Jonker, P.G., Juhász, Á.L., Julbe, F., Karampelas, A., Kewley, A., Klar, J., Kochoska, A., Kohley, R., Kolenberg, K., Kontizas, M., Kontizas, E., Koposov, S.E., Kordopatis, G., Kostrzewa-Rutkowska, Z., Koubzsky, P., Lambert, S., Lanza, A.F., Lasne, Y., Lavigne, J.B., Le Fustec, Y., Le Poncin-Lafitte, C., Lebreton, Y., Leccia, S., Leclerc, N., Lecoœur-Taïbi, I., Lenhardt, H., Leroux, F., Liao, S., Licata, E., Lindstrøm, H.E.P., Lister, T.A., Livanou, E., Lobel, A., López, M., Managau, S., Mann, R.G., Mantelet, G., Marchal, O., Marchant, J.M., Marconi, M., Marinoni, S., Marschalkó, G., Marshall, D.J., Martino, M.,

- Marton, G., Mary, N., Massari, D., Matijević, G., Mazeh, T., McMillan, P.J., Messina, S., Michalik, D., Millar, N.R., Molina, D., Molinaro, R., Molnár, L., Montegriffo, P., Mor, R., Morbidelli, R., Morel, T., Morris, D., Mulone, A.F., Muraveva, T., Musella, I., Nelemans, G., Nicastrò, L., Noval, L., O'Mullane, W., Ordóñez-Blanco, D., Osborne, P., Pagani, C., Pagano, I., Paillet, F., Palacin, H., Palaversa, L., Panahi, A., Pawlak, M., Piersimoni, A.M., Pineau, F.X., Plachy, E., Plum, G., Poggio, E., Prša, A., Pulone, L., Racero, E., Ragaini, S., Rambaux, N., Ramos-Lerate, M., Regibo, S., Reylyé, C., Riclet, F., Ripepi, V., Riva, A., Rivard, A., Rixon, G., Roegiers, T., Roelens, M., Romero-Gómez, M., Rowell, N., Royer, F., Ruiz-Dern, L., Sadowski, G., Sagristà Sellés, T., Sahlmann, J., Salgado, J., Salguero, E., Sanna, N., Santana-Ros, T., Sarasso, M., Savietto, H., Schultheis, M., Sciacca, E., Segol, M., Segovia, J.C., Ségransan, D., Shih, I.C., Siltala, L., Silva, A.F., Smart, R.L., Smith, K.W., Solano, E., Solitro, F., Sordo, R., Soria Nieto, S., Souchay, J., Spagna, A., Stampa, U., Steele, I.A., Steidelmüller, H., Stephenson, C.A., Stoev, H., Suess, F.F., Surdej, J., Szabados, L., Szegedi-Elek, E., Tapiador, D., Taris, F., Tauran, G., Taylor, M.B., Teixeira, R., Terrett, D., Teysandier, P., Titarenko, A., Torra Clotet, F., Turon, C., Ulla, A., Utrilla, E., Uzzi, S., Vaillant, M., Valentini, G., Valette, V., van Elteren, A., Van Hemelryck, E., van Leeuwen, M., Vaschetto, M., Vecchiato, A., Veljanoski, J., Viala, Y., Vicente, D., Vogt, S., von Essen, C., Voss, H., Votruba, V., Voutsinas, S., Weiler, M., Wertz, O., Wevers, T., Wyrzykowski, L., Yoldas, A., Žerjal, M., Ziaeeppour, H., Zorec, J., Zschocke, S., Zucker, S., Zurbach, C., Zwitter, T.: Gaia Data Release 2. Observations of solar system objects. *A&A* **616**:A13 (2018b)
- Galushina, T.Y., Sambarov, G.E.: Dynamics of Asteroid 3200 Phaethon Under Overlap of Different Resonances. *Solar System Research* **53**(3), 215–223 (2019)
- Greenberg, A.H., Margot, J.L., Verma, A.K., Taylor, P.A., Hodge, S.E.: Yarkovsky Drift Detections for 247 Near-Earth Asteroids. *AJ* **159**(3):92 (2020)
- Jones, D.L., Folkner, W.M., Jacobson, R.A., Jacobs, C.S., Dhawan, V., Romney, J., Fomalont, E.: Astrometry of Cassini with the VLBA to improve the Saturn ephemeris. *The Astronomical Journal* **149**(1), 28 (2014)
- Mouret, S., Hestroffer, D., Mignard, F.: Asteroid mass determination with the Gaia mission. A simulation of the expected precisions. *Planet. Space Sci.* **56**(14), 1819–1822 (2008)
- Vereš, P., Farnocchia, D., Chesley, S.R., Chamberlin, A.B.: Statistical analysis of astrometric errors for the most productive asteroid surveys. *Icarus* **296**, 139–149 (2017)
- Verma, A.K., Fienga, A., Laskar, J., Issautier, K., Manche, H., Gastineau, M.: Electron density distribution and solar plasma correction of radio signals using MGS, MEX, and VEX spacecraft navigation data and its application to planetary ephemerides. *A&A* **550**:A124 (2013)
- Verma, A.K., Fienga, A., Laskar, J., Manche, H., Gastineau, M.: Use of MESSENGER radioscience data to improve planetary ephemeris and to test general relativity. *A&A* **561**:A115 (2014)
- Verma, A.K., Margot, J.L., Greenberg, A.H.: Prospects of Dynamical Determination of General Relativity Parameter β and Solar Quadrupole Moment J_2 with Asteroid Radar Astronomy. *ApJ* **845**(2):166 (2017)
- Viswanathan, V.: Improving the dynamical model of the Moon using lunar laser ranging and spacecraft data. Phd thesis, Observatoire de Paris (2017)

-
- Vokrouhlický, D., Milani, A., Chesley, S.R.: Yarkovsky Effect on Small Near-Earth Asteroids: Mathematical Formulation and Examples. *Icarus* **148**(1), 118–138 (2000)
- Zhang, F. (2005) *The Schur Complement and its Applications, Numerical Methods and Algorithms*, vol 4. Springer, New York, DOI 10.1007/b105056